Materials Horizons

Understanding, Quantifying, and Controlling the Molecular Ordering of Semiconducting Polymers: From Novices to Experts and Amorphous to Perfect Crystals

Journal:	*Materials Horizons*
Manuscript ID	MH-REV-05-2020-000837.R3
Article Type:	Review Article
Date Submitted by the Author:	30-Nov-2021
Complete List of Authors:	Peng, Zhengxing; North Carolina State University, Ye, Long; Tianjin University, materials science and engineering; North Carolina State University, physics Ade, Harald; North Carolina State University, Physics

Understanding, Quantifying, and Controlling the Molecular Ordering of Semiconducting Polymers: From Novices to Experts and Amorphous to Perfect Crystals

Zhengxing Peng, Long Ye[§,]*, Harald Ade*

Department of Physics and Organic and Carbon Electronics Laboratories (ORaCEL), North Carolina State University, Raleigh, North Carolina 27695, United States

* E-mail: hwade@ncsu.edu

[§]Current address: School of Materials Science & Engineering and Tianjin Key Laboratory of Molecular Optoelectronic Sciences, Tianjin University, Tianjin 300350, P.R. China

* E-mail: yelong@tju.edu.cn

Abstract: Molecular packing and texture of semiconducting polymers are often critical to the performance of devices using these materials. Although frameworks exist to quantify the ordering, interpretations are often just qualitative, resulting in imprecise use of terminology. Here, we reemphasize the significance of quantifying molecular ordering in terms of degree of crystallinity (volume fractions that are ordered) and quality of ordering and their relation to the size scale of an ordered region. We are motivated in part by our own imprecise and inconsistent use of terminology in the past, as well as the need to have a primer or tutorial reference to teach new group members. We strive to develop and use consistent terminology with regards to crystallinity, semicrystallinity, paracrystallinity, and related characteristics. To account for vastly different quality of ordering along different directions, we classify paracrystals into 2D and 3D paracrystals and use paracrystallite to describe the spatial extent of molecular ordering in 1-10 nm. We show that a deeper understanding of molecular ordering can be achieved by combining grazing-incidence wide-angle X-ray scattering and differential scanning calorimetry, even though not all aspects of these measurements are consistent, and some classification appears to be method dependent. We classify a broad range of representative polymers under common processing conditions into five categories based on the quantitative analysis of the paracrystalline disorder parameter (g) and thermal transitions. A small database is presented for 13 representative conjugated and insulating

polymers ranging from amorphous to semi-paracrystalline. Finally, we outline the challenges to rationally design more perfect polymer crystals and propose a new molecular design approach that envisions conceptual molecular grafting that is akin to strained and unstrained hetero-epitaxy in classic (compound) semiconductors thin film growth.

1. Introduction and overview

In the past two decades, thousands of new π-conjugated materials have been reported and used in organic electronic devices. Conjugated polymers are those with alternating π and σ bonds leading to π-orbital overlap to create delocalized π-electrons, exhibiting semiconductivity and interesting optoelectronic properties. Polymer semiconductors offer great opportunities and potentials due to their light weight, color tunability, mechanic flexibility and the ability to be deposited on large-area flexible substrates at low cost. They have been targeted as active materials for a range of electronic applications, such as organic field-effect transistors for flexible circuity, logic circuit and sensor[1, 2], organic light-emitting diodes for display applications[3], organic solar cells (OSCs) for energy harvesting[4] including semitransparent building[5] and greenhouse integration[6], and organic electrochemical transistors for bioelectronics in biosensors and neural implants[7, 8]. Conjugated polymers are gaining particular attention in bioelectronics due to their similarities in chemical properties (such as soft/compliant and ion/electron conducting) with biological molecules and capacity to be engineered in various forms. They find application in wearable health monitor for heart disease (blood, oxygenation, pulse, enzyme, *etc.*)[9] and diabetes (blood sugar sensors, sweat sensors)[10], and neuronal therapies (including recording and stimulating neural activity, the regeneration of neural tissue and the delivery of bioactive molecules for mediating device–tissue interactions)[8, 9, 11-13]. An additional emergent application is their use in neuromorphic computing[14, 15].

The intrinsic structural properties of polymer chains, such as different degrees of conformational and configurational freedom and chain stiffness, determine how crystalline or amorphous the polymeric materials are intrinsically and how important kinetic factors are in impacting ordering in specific fabrication procedures[16, 17]. The perfection of the ordering is determined by the local molecular packing, and the resulting ordered or disordered films and their texture affect optical

absorption, exciton delocalization, charge separation, and charge transfer. In contrast to small molecules, it is currently impossible for conjugated polymers to have a high degree of crystallinity (DoC) (*i.e.*, high volume fraction of crystalline/paracrystalline ordering) or be perfectly packed (*i.e.*, crystals have high quality of ordering). Polymers are generally only semicrystalline and paracrystalline (except for some liquid crystalline polymers), respectively, as illustrated in **Figure 1a** and **Figure 1c.** Here, 'semi-' refers to 'partially crystalline' or 'partially paracrystalline' when the DoC is limited and there is generally an amorphous or disordered volume fraction even in the most highly ordered materials due to crystallization kinetics and the covalent constraint along the backbone. 'Para-' refers to the imperfect molecular ordering when ordered domains are generally paracrystalline with cumulative rather than random lattice distortions (**Figure 1b)**, as illustrated schematically in **Figure 1c**. The molecular design differentiates ordering along three directions: π-π stacking direction, lamellar stacking direction, and backbone chain direction, as illustrated in **Figure 1e.** It should be noted that these three directions are not necessarily perpendicular to each other, depending on the types of unit cells. Given that the coherence length (L_c), a measure of the size of the coherently diffracting regions (*e.g.*, a crystallite or a domain), might be different in these three directions, one could or maybe should conceptually think of the spatial extent of the primary ordered region to be represented and approximated by a coherence ellipsoid, shown in **Figure 1f**. The coherence ellipsoid is proposed to illustrate the anisotropy of L_c in these three directions in a Cartesian coordinate which does not imply these three directions to be perpendicular to each other. When there is no manifest ordering, the conjugated polymers are amorphous, and the coherence ellipsoid is very small in all directions. Conversely, highly asymmetric ellipsoids represent ordering in reduced dimensions, such as a 2D crystal. Due to the frequent difficulty in determining this ellipsoid particularly along the backbone direction and differentiating the contribution to peak broadening from crystal size, cumulative and non-cumulative lattice disorder, materials and samples are often identified and reported in the literature simply as semicrystalline or amorphous. Sometimes, the terminology is not well defined and not consistent across the literature. For example, the benchmark and widely studied polymer PTB7 (full name see **appendix A**) of interest in solar cells was reported to be semicrystalline in several papers[18, 19] because of the presence of (100) and (010) peaks in the X-ray diffraction patterns, while in other papers PTB7 was considered amorphous[20, 21] due to the lack of the long-range order and lack of higher order diffraction peaks. Whatever the cause of this inconsistency and given existing basic IUPAC

definitions[22] and prior work utilizing the Warren-Averbach framework[23, 24], it is highly desirable that a more consistent terminology be used even when only semi-quantitative analysis is performed.

To help guide and encourage the development and use of more precise terminology, we discuss the molecular ordering of conjugated polymers undergoing common processing histories to range from amorphous to semi-paracrystalline (account for both the limited DoC and imperfect molecular ordering) in a quantitative manner by combining both grazing-incidence wide-angle X-ray scattering (GIWAXS)[25] and differential scanning calorimetry (DSC). We note and stress the importance of the processing history and batch-to-batch variation on the packing, texture, and degree of ordering of the polymers. We are less interested in the intrinsic properties in the thermodynamic limit and more interested in a given sample or device than the material *per se*. We will focus on a given ***packing state*** that is determined by the processing and application we have at hand, for example, the active layer in an OSC cast with a material of a certain molecular weight from a particular solvent. This mirrors non-organic materials and their nomenclature, where silicon can be crystalline (c-Si) or amorphous (a-Si) depending on the processing history.

We dedicate Section 2 of this review to the delineation of important concepts and labels such as crystals, crystallites, aggregate, and crystallinity in polymeric semiconducting materials, and introduce some quantitative parameters of molecular order derived from GIWAXS and DSC. Chiefly among them is the paracrystalline disorder parameter (g), which quantifies the cumulative lattice distortions that prevent long-range order. We aim to clarify the transition from amorphous to semi-paracrystalline by comparing various semiconducting polymeric thin films to the classic amorphous polystyrene (PS) and poly(methyl methacrylate) (PMMA). In Section 3, we propose to classify polymers into five basic categories, 3D amorphous, oriented amorphous, highly disordered, 2D semi-paracrystalline (2D paracrystallites), and 3D semi-paracrystalline (3D paracrystallites), to capture differences based on the g parameter associated with (h00) and (0k0) peaks, thermal characteristics, and general microscopy observations. Here, '2D' refers to paracrystallinity in only two dimensions (*i.e.*, g parameter indicating amorphous disorder in at least one dimension) while '3D' refers to g parameters < 12% in all three directions. The label semicrystalline/crystalline (crystallites) is reserved for materials with long-range order with g < 2% in all directions. We discuss the current use of a-Si as a reference (with g = 12%) to define the boundary between amorphous and paracrystalline. We have not resolved all nomenclature issues,

something that might have to be taken up by the IUPAC at some point. We also provide examples of a broad range of representative polymers with typical processing histories into these five proposed categories and advocate use of a consistent nomenclature for differentiation along with publishing, whenever possible, the *g* parameters and DoC.

In Section 4, we discuss the challenges and possible solutions to create large crystals with low structural disorder and high DoC, *i.e.,* "perfect crystals", which is an essential way to improve exciton diffusion length and enhance charge mobility. For these challenges, we focus on recent work[26] that clearly indicates that sidechain ordering and backbone ordering is generally not synergistic, a competition that is likely at the very core of semiconducting polymers exhibiting generally large *g* parameters of > 6%. Questions naturally arise as to what it would take to achieve nearly perfect crystals of semiconducting polymers with disorder that approaches that of TIPS-pentacene ($g < 4\%$). Highly ordered materials with long-range ordering and low *g* parameter would likely require special molecular design that could be guided by the conceptual hetero-epitaxy grafting design method proposed in this review.

Overall, we provide clarification of key terms related to molecular ordering in conjugated polymers to help use of consistent terminology in the field, classify common polymer thin films into five proposed categories, and discuss possible solution to reach perfect crystals.

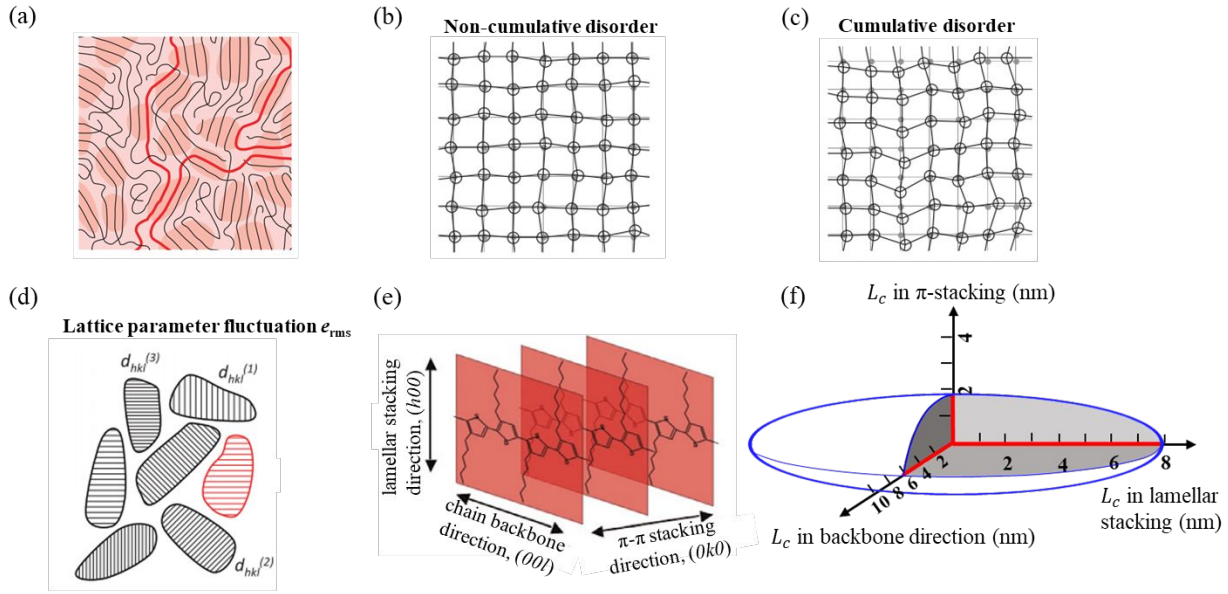

Figure 1. a) Schematic illustration of the complicated nature of conjugated polymers[27]. Reproduced with permission from ref. 27. b) Schematic illustration of random Gaussian (noncumulative) and c) paracrystalline (cumulative) disorder in a 2D lattice[24]. Reproduced with permission from ref. 24. d) Schematic illustration of lattice parameter fluctuation e_{rms}, showing a slight variation of the interplanar distance d_{hkl} from one crystallite to another. Reproduced with permission from ref. 24. e) Typical schematic of the packing structure of an ordered conjugated polymer (P3HT)[28] that generally assumes orthorhombic unit cells and that may be ordered in up to three directions: π-π stacking direction, lamellar stacking direction, and chain backbone direction. Adapted with permission from ref. 28. f) Illustration of coherence ellipsoid that the coherence length is often different in different packing directions with an example of PM6 which shows coherence length (L_c) of 7.9 nm, 1.8 nm, 6.3 nm in lamellar-stacking, π-stacking, backbone directions, respectively.

2. Quantification of Molecular Order and Related Terminologies

In this section, we will first provide some examples of terminology miscues, then delineate key terms (crystallites/aggregate, DoC, paracrystalline, amorphous), provide a brief introduction of the two main characterization techniques used for molecular ordering characterization (GIWAXS and DSC), and finally provide a framework that can be derived from these measurements.

2.1 Clarifications of the Key Concepts and Nomenclature Related to Molecular Order

Terminology miscues

In the semiconducting polymer literature, using the term "crystallinity" without qualifiers is often confusing because two different concepts, the DoC and quality of ordering within a crystallite, are generally undifferentiated and mixed up. What does it really mean if a material is declared "highly crystalline"? In principle, referring to just "crystallinity" without qualifiers works if the quality of the ordered regions and volume fractions of ordered regions are highly correlated. Though such correlation is common for inorganic materials and some crystallizable small molecules, such correlation is not assured for semiconducting polymers. The quality of the ordered regions can be high, while their volume fraction can be low (if, for example, only a few crystals were nucleated).

Or the converse is possible: the quality of the ordered regions is very low, but the volume fraction is very high (*e.g.*, classic paracrystallinity[29]).

Despite the known high disorder in semiconducting polymers[27], reference to "crystallinity" is often misused to describe the quality of ordering, rather than the most recognized referring to DoC. For example, when analyzing and discussing the GIWAXS data, it was claimed that the presence of two scattering peaks, namely the so-called lamellar (100) peak and (010) π-π stacking peak, of PBDT-TDZ and PBDTS-TDZ films showed their "crystallinity nature"[30]. Sometimes, "crystallinity" is used to even refer to spacing. For example, it was reported[30] that "the shorter π-stacking distance of PBDTS-TDZ than PBDT-TDZ indicates a better crystallinity of PBDTS-TDZ". Or the observed (001) peak indicated the excellent crystallinity of P(NDI2OD-T2) when processed with 2-methyltetrahydrofuran[31]. Such use is prevalent, even in cases where DSC cannot detect a melting peak and when the volume fraction of ordered material might be very small. We do not intend to single out anybody with these specific examples and point out our own prior miscues of terminology in a similar way[32-35]. We simply want to provide examples and encourage a dialog in the field about these issues.

Quality, quantity and size scale of ordered regions

In solid state matter, a single crystal is defined to be a periodic array of identical motifs filling the space, having a long-range positional order of the atomic length scale in three-dimensional space. However, in polymeric materials, three-dimensional order is almost impossible and long-range periodicities might be lacking in at least one dimension[16]. Also, there always exists structural disorder, paracrystallinity or defects inside polymeric crystals, and thus polymeric materials are never completely crystalline, but semicrystalline, paracrystalline, or amorphous instead. They might even be nano-layered with alternating ordered or disordered sidechain or backbone layers (see section 4.2)[26]. Generally, amorphous materials exhibit a glass transition temperature (T_g) that can be revealed with thermal or thermo-mechanical measurements. Semicrystalline materials exhibit a T_g in addition to a melting temperature (T_m), but classic paracrystalline materials only exhibit a T_m[29]. Structural and thermal measurements are thus excellent complements to each other.

To describe the molecular ordering comprehensively, we need to separate the concepts of quality of ordering, degree of ordering, and spatial extent of the ordered region. In short, we need to differentiate the ***quality***, ***quantity*** and ***size scale*** of the ordered regions. We will focus on quality

and quantity in detail, but also discuss size scale. Some of the more subtle issues regarding size scale remain unresolved, due to the underlying complexity and remaining ambiguities.

Let us begin by examining current terminology associated with size scale. Since the ordered phase in a typical semicrystalline polymer film is on the order of 1-100 nm in diameter or thickness[23], such ordered regions are usually called crystallite rather than crystal. Aggregate is also used frequently to describe ordered regions, while its definition is somewhat vague and needs to be clarified. In a broad sense, 'aggregate' refers to spatial clustering of the material without explicit or implicit references to specific characteristics. We note that such structural aggregates need to be clearly distinguished from optical aggregates where the coupling is not by a force, but between optical dipoles via the electromagnetic field[36, 37]. In the X-ray diffraction view, D. T. Duong *et al.*[38, 39] defined an "aggregate" as a group of the π-stacked conjugated segments with the lack of the lamellar stacking. With enough π-stacked conjugated segments, aggregates can also produce discernible diffraction peaks. R. Noriega *et al.*[27] also proposed that small semi-ordered domains with short-range ordering of a few molecular units to be referred to as aggregates, compared to the crystallites with larger domains and with better three-dimensional long-range periodicity. Short-range ordered aggregates often yield sufficient π-orbital overlap[36, 40] to facilitate interchain charge transport, resulting in some seemingly contradictory cases where the polymers show a less ordered lamellar packing structure but excellent charge transport properties[27]. Based on existing polymer physics concepts reaching back to the 1960s, we will use a different terminology below, after we have fully delineated paracrystallinity and understand better if and how size, quality and quantity can be determined.

Next, we consider the quantity of ordering. Since there exist both ordered and disordered or amorphous regions, the fraction of crystalline/paracrystalline to amorphous regions is a critical parameter quantifying how much a polymer is ordered. The DoC is defined as the volume fraction of crystalline or paracrystalline material in a film[23]. We will describe methods below how the DoC can be determined.

The quality of molecular ordering is typically assessed with X-ray diffraction methods. These will be discussed in detail below. If the local order is so short-ranged that only one diffraction order is observed and the ordering cannot be detected by observing a T_m, but rather a T_g is detected in DSC, the samples are identified and classified as amorphous. This condition generally correlates with *g*

parameters that are indicating amorphous characteristics ($g > 12\%$). The central discussions about paracrystalline *g* parameter draw heavily on well understood X-ray scattering concepts that have been previously delineated by the Salleo group[23, 24, 27].

One of the miscues seems to be that authors infer "crystalline"/ "semicrystalline" due to the presence of a single scattering peak. It is impossible though to make a polymer thin film with completely random distances and orientation, and without any molecular correlations between nearest molecular neighbors. Only a gas would exhibit randomness with a *g* parameter of 100%. In a completely amorphous (random) liquid or glassy semiconducting polymer that is highly disordered, nearest chain distances still correlate locally without constituting a distinct ordered phase. Due to these local correlations, even classic amorphous polymers, such as atactic polystyrene (PS) and poly (methyl methacrylate) (PMMA), tend to scatter diffusely in X-ray diffraction experiments with broad scattering peaks corresponding to nearest neighbor distances. We will show below that the diffraction or scattering peaks in PMMA and PS are qualitatively very similar to the scattering characteristics of many semiconducting polymers and observation of such peaks is thus not a qualifying characteristic for paracrystallinity, let alone crystallinity.

Mesoscale ordering

In addition to the molecular level packing that defines paracrystalline and amorphous properties, there is an important level of ordering in semiconducting polymers on the mesoscale: liquid crystalline ordering.

Liquid crystals are materials that have the properties of both a crystal and a liquid, which lies in an intermediate state between the isotropic amorphous liquid state and crystalline state. The liquid crystals do not show the 3D positional order of crystals but retain some orientational order. The main characteristics that make liquid crystalline ordering unique and distinct from crystalline structure is that the exothermic or endothermic enthalpy for crystallization or melting of liquid crystals is generally independent of the cooling/heating rate[41]. For semiconducting polymers, there are some polymers that can exhibit liquid crystalline properties, such as fluorene copolymers (F8BT, F8T2)[42], polyalkylidene fluorene[43], PQT[44], PCDTBT[45], PBTTT[41, 46]. X. Zhang *et al.*[46] have demonstrated via dark-field transmission electron microscopy (TEM) orientation map that PBTTT crystallite orientation varies smoothly across relatively large distances, with only small angle variations between adjacent diffracting regions. This in-plane, liquid crystalline texture helps to

decrease the density of abrupt grain boundaries, leading to excellent thin-film transistor device properties. We note that in this case, DSC can readily identify two melting transitions as expected for the presence of an LC phase. Soft x-ray scattering with polarized radiation (P-SoXS) can assess with high orientational sensitivity mesoscale ordering in the 20-2,000 nm range and has observed such characteristics even in as-cast PBTTT films where TEM analysis was inconclusive[47, 48]. Length scales of >30 nm can be also readily probed with dichroic scanning transmission x-ray microscopy[49, 50]. R. Xie *et al.*[45] reported the nematic ordering for PFTBT and PCDTBT by a combination of DSC, temperature-dependent x-ray scattering and linear viscoelastic rheology. The local chain alignment via the nematic order can reduce the chain entanglement, leading to faster chain relaxation from the topological constraints of surrounding chains. We will not focus on liquid crystalline ordering in this review and mention only briefly these properties to provide completeness.

2.2 GIWAXS and DSC: Complementary Tools

X-ray diffraction is a non-destructive technique to characterize molecular packing in a material and determine unit-cell parameters, DoC, anisotropy/texture, and lattice disorder. X-ray diffraction experiments of typical semiconducting polymer thin films are generally synchrotron-based for reduced collection time and sufficient signal-to-noise ratio although some in-house, lab-based X-ray measurements can be performed for strongly scattering films. In a GIWAXS measurement, the X-ray beam is incident on the sample at a shallow angle as shown in **Figure 2a**. This angle is typically close to the critical angle and can be adjusted to control how deep the X-rays penetrate the film or tuned to a wave guide resonance for boosting the scattering intensity[51]. Constructive interference, governed at a fundamental level by Bragg's law, results in observable diffraction peaks on a 2D detector from ordered materials. Disordered materials produce a diffuse halo. The peak location can be used to calculate interplanar spacings in the material. The integrated peak intensity of ordered regions after resolution function correction encodes the DoC for fiber texture[23] (the texture with only out-of-plane orientation preference but no in-plane orientation preference), which is often the case in semiconducting polymers. The peak width and shape are determined by the crystal size, cumulative or noncumulative lattice distortions, and lattice parameter fluctuations. We will discuss the most salient aspects of these concepts below, but due to space limitations we

would like to refer the readers interested in additional details to excellent monographs and prior reviews[23, 52, 53].

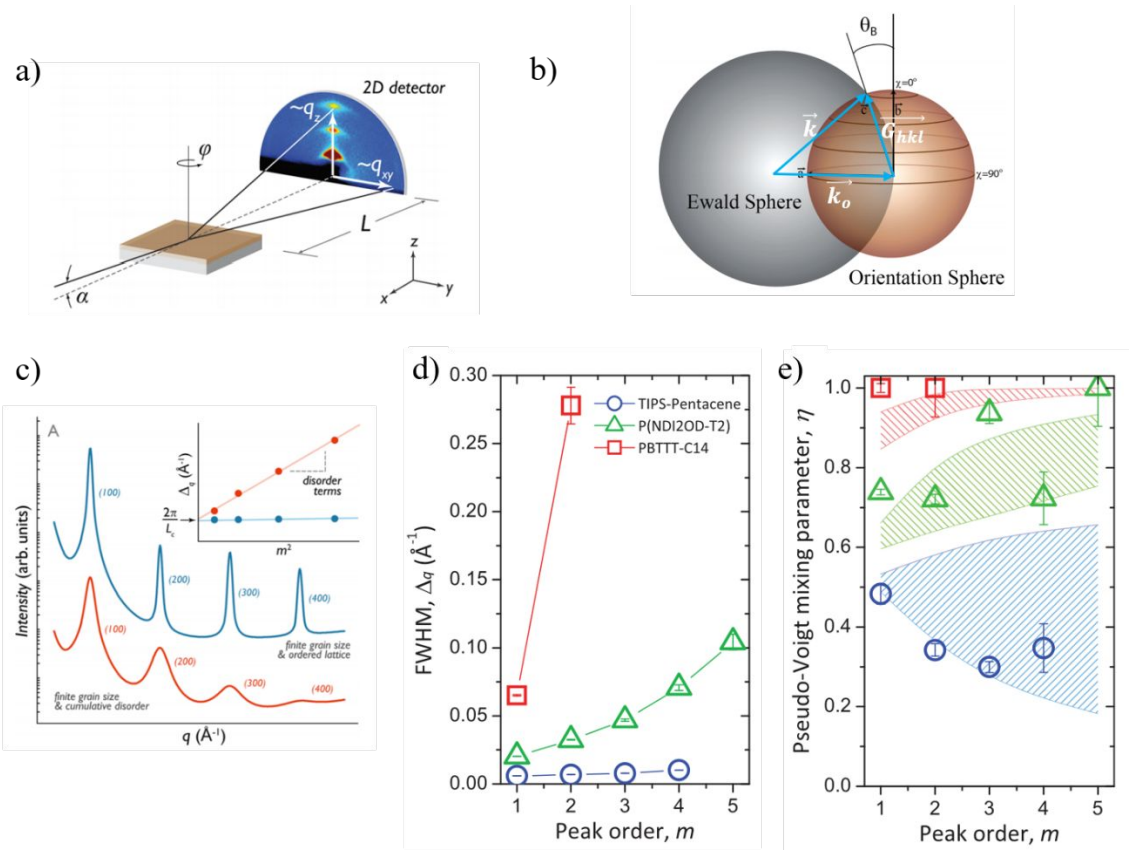

Figure 2. a) Schematic of GIWAXS measurement setup[23]. Reproduced with permission from ref. 23. b) Intersection of Ewald sphere with a given crystallite orientation sphere which is oriented perpendicular to the substrate with the radius defined by the $\overrightarrow{q_B}$ of interest. $\overrightarrow{k_o}$ is the incoming vector, $\vec{k}$ is the diffracted vector, $\overrightarrow{q_B}$ is the scattering vector of interest defined by $\overrightarrow{q_B} = \vec{k} - \overrightarrow{k_o}$, and $\overrightarrow{G_{hkl}}$ is the reciprocal lattice vector to the plane (*hkl*) of the oriented crystallite. Bragg's law can be satisfied when the Ewald sphere intersects with the crystallite orientation sphere, that is when $\overrightarrow{q_B} = \vec{k} - \overrightarrow{k_o} = \overrightarrow{G_{hkl}}$, and thus this construction indicates possible diffraction events in grazing incidence geometry[54]. Adapted with permission from ref. 54. c) Schematic of hypothetical diffraction profile from crystalline lattices affected by finite size with (red) and without (blue) the contribution of cumulative disorder[23]. Inset: The contribution of cumulative disorder results in an increasing peak width (red) while the absence of it gives a constant peak width (blue). Reproduced with permission from ref. 23. d) FWHM of diffraction peak and e) pseudo-Voigt mixing parameter as a function of peak order for TIPS-pentacene (blue circle), P(NDI2OD-T2) (green triangle), and PBTTT (red square)[24]. Reproduced with permission from ref. 24.

A useful tool to determine the observable constructive interference is the Ewald sphere, which is constructed with its radius defined by the incoming $\overrightarrow{k_o}$ vector and centered at the origin of $\overrightarrow{k_o}$. For a given oriented crystallite, when a reciprocal lattice point in the crystallite orientation sphere intersects with Ewald sphere, diffraction takes place with Laue condition that the scattering vector $\overrightarrow{q_B}$ ($\equiv \vec{k} - \overrightarrow{k_o}$) is equal to the reciprocal lattice vector $\overrightarrow{G_{hkl}}$[55], as illustrated in **Figure 2b**. In this way, the intersection of the Ewald sphere with a given crystallite orientation sphere indicates possible diffraction events[54]. It should be noted that the crystallites with $\overrightarrow{q_B}$ close to the substrate normal will not intersect the Ewald sphere and do not result in observed diffraction in GIWAXS setup. Due to the q_z component needed to get onto the Ewald sphere, the scattering intensity collected with a flat 2D detector in grazing incidence geometry is distorted with the result that the detector image is not a direct q_x-q_y map of reciprocal space. This distortion can be corrected, leading to the so-called missing wedge in the corrected 2D pattern that corresponds to q_x-q_y combinations without Ewald sphere intersections. The reader is referred to the literature[56] for more details about this correction. If the substrate is tilted at θ_B (denoted in **Figure 2b**), the local specular condition can be met[54]. A pole figure is a plot that shows the orientation distribution of a certain Bragg reflection and provides information on the texture of thin films. A correct pole figure is the product of the sine of the azimuthal angle (χ, defined as the angle between the crystallite orientation and the substrate normal) and the measured intensity at this azimuthal angle[57], which is the so-called sin(χ) correction or Ewald sphere correction. Since the Ewald sphere cannot intersect the orientation sphere with the perpendicular direction in grazing geometry, a complete pole figure can only be reached by combining the data from the grazing patterns with the local specular diffraction pattern with the substrate tilted with θ_B[54].

Before we go into more details about GIWAXS analysis, it is necessary to provide some discussion about the unit cell determined from the X-ray diffraction. In most cases, it is usually assumed without justification and mostly because of a lack of sufficient diffraction information that the lattice packing in conjugated polymers is orthorhombic. However, some polymers are reported to pack in triclinic with off-axis peaks present, such as PBTTT[58], P3EHT[59], PQT[60]. The determination of unit cell parameters requires careful crystallographic X-ray analysis and the reader is referred to the literature[61, 62] for details. Generally, in orthorhombic unit cell, the off-axis, mixed-index peaks (*hkl*) are aligned horizontally relative to the (*h*00) peaks. For example, (*h*00) and (*h*01) have

the same q_z since the (h00) and (00l) planes are orthogonal assuming c□ is normal to the film substrate. However, in triclinic cells, the (h00) planes can be non-orthogonal to the (00l) planes. The presence of off-axis peaks signifies coherent three-dimensional molecular packing.

As a key complement to GIWAXS, DSC is a thermal analysis technique characterizing how a material's heat capacity is changed with temperatures. Different from GIWAXS measurements, which are performed on spun-cast thin films of uniform thickness, conventional DSC measurement is normally conducted with bulk powders or drop cast films. To obtain information on spun-cast thin films, which tend to be more disordered than drop-cast films, flash DSC can be utilized. DSC is generally applied to detect thermal transitions such as the glass transition (T_g), crystallization (T_c) and melting (T_m) associated with disordered and ordered phases of the sample. In general, the smaller the highly ordered crystallite (*e.g.*, P3HT), the lower the melting temperature. In addition to the phase transition temperatures, DSC can also record the exothermic or endothermic enthalpy associated with crystallization and/or melting. The enthalpy is obtained by integrating the DSC signal over the appropriate temperature range with proper background subtraction. Generally, the enthalpies can be used to infer the degree of ordering between samples of the same material. Conventional DSC can only be performed below the decomposition temperature of a material.

There currently exists a conundrum between the GIWAXS and DSC results for some materials. When the quality of ordering is low, the melting of paracrystalline domains cannot always be detected while GIWAXS and microscopy indicate the presence of some kind of ordered domains. Use of a flash-DSC, which achieves much higher sensitivity to heat flow, can go to higher temperatures than conventional DSC, and investigate identical spun-cast films, might be able to reconcile these differences in the future. We are of the opinion that the determination of paracrystalline or amorphous characteristics should not depend strongly on the characterization methods and hope that the remaining differences can be reconciled.

Other techniques are capable of characterizing certain aspects of molecular order, like nuclear magnetic resonance (NMR) or mass density measurements. With ^{13}C solid state NMR, the conformational states of backbone or side chain for a certain carbon belonging to ordered or disordered fractions can be separated. Generally, it requires a relatively large fraction of the available materials (often tens of mg with typical synthetic batches yielding ~50 mg), and it is not

very compatible with the thin film form factor, *i.e.*, spun-cast thin films, used in GIWAXS. Moreover, it is challenging to identify the molecular origins of NMR peaks and the subtle difference in ordered or disordered phases. As a result, NMR use has been limited to a few studies. The mass density or specific volume depends on the crystalline/paracrystalline and amorphous/disordered volume fraction of a material, and thus mass density determined with density gradient column can be applied to characterize the DoC of a semicrystalline film, but not the quality of the molecular ordering. Therefore, in this article, the discussion of NMR and mass density measurements and their applications are limited.

2.3 Quantitative Characterization of Molecular Order

Parameters characterizing molecular packing

To quantitatively characterize the ordering of a material and the properties of the molecular packing, the most critical aspects may include: 1) the unit cell, 2) the **quality** of the molecular packing (*e.g.*, the types of disorder), 3) the DoC (**quantity**), 4) the texture of the packing (*e.g.*, molecular orientation distribution), and 5) the **size** of the molecularly ordered regions. We will focus mainly on the **quality, quantity, and size scale** (crystallite size or coherence length of coherently diffracting regions). These are interrelated in the measurements and need to be disentangled. The parameters that can be directly quantified from GIWAXS are the *d*-spacing, coherence length (L_c), pseudo-Voigt mixing parameter (η), and rDoC (relative DoC) since these can be extracted from a single peak. In favorable situations of at least three orders of diffraction peaks, the paracrystalline disorder parameter (g), lattice parameter fluctuation (e_{rms}), and crystallite size (if it has) can also be determined. In some circumstances and with certain assumptions, the g parameter can be estimated from a single peak. The melting enthalpy (ΔH) from DSC can provide rDoC. Recalling concepts delineated in **Figures 1b-e** and **2c-e**, a road map about how to relate these parameters to the packing properties and the conditions needed to extract them from the data is summarized in **Scheme 1**.

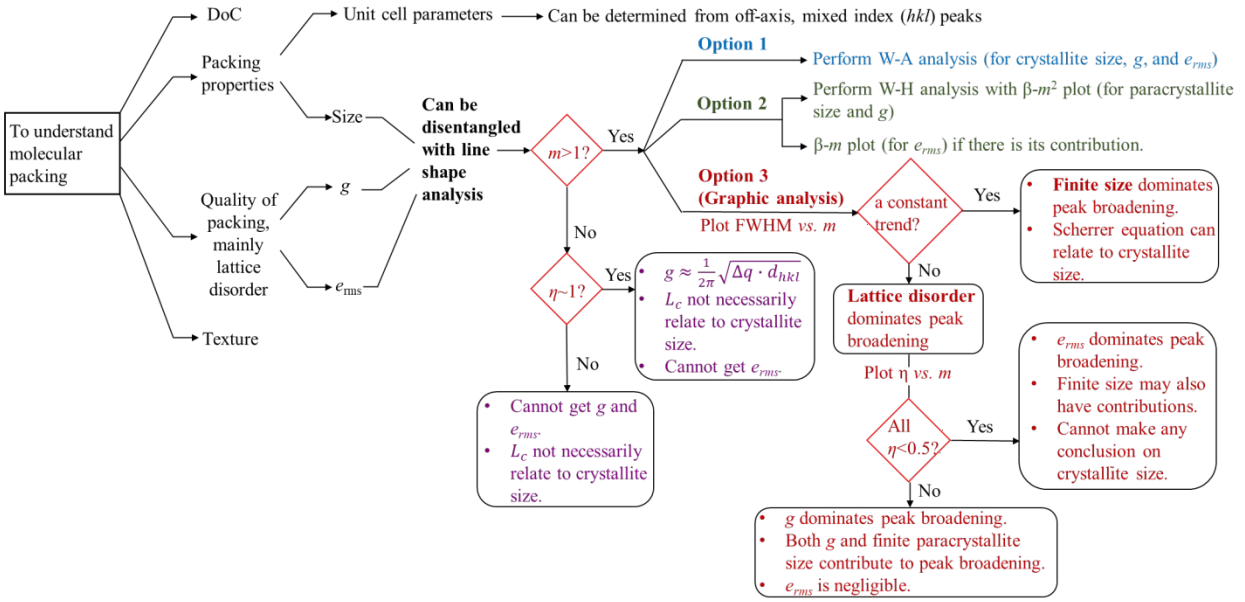

Scheme 1. A road map summarizing the aspects and parameters needed to understand the molecular packing where m is referring to the peak order. To disentangle the contribution from finite size, paracrystalline disorder parameter (g), and lattice parameter fluctuation (e_{rms}) to the peak broadening, with the presence of higher ordered peaks ($m > 1$), there are three options: performing W-A analysis for comprehensive analysis (option 1); performing W-H analysis with β-m^2 plot to obtain the g parameter and paracrystallite size or perform β-m plot for e_{rms} (option 2); or plotting FWHM/η *vs*. m for graphical analysis (option 3). When there is only the first order peak presented (m=1), g parameter can be estimated with some assumption if η is close to 1.

The interplanar spacing, or d-spacing, of a certain diffraction peak, such as lamellar stacking peak or π-π stacking peak, can be calculated from the reciprocal of the peak position with $d = \frac{2\pi}{q}$. A commonly used method to determine the crystallite size is use of the Scherrer equation[63], which relates the peak width and crystallite size via $L_c = \frac{2\pi K}{\Delta q}$, where Δq is the full width at half maximum (FWHM) of the peak and K is the shape factor account for the different crystallite shapes (*e.g.*, sphere, cube, octahedra). In most cases the actual crystallite shape is either unknown or ill defined, and thus it is common practice to use a typical value of ~0.9[64], which is also used in **Table** 1. The Scherrer equation estimates the crystallite size with the assumption that the crystallite size is the main contributor to the broadening of the diffraction peaks. This assumption is generally not met

since paracrystalline disorder and lattice parameter fluctuation can also contribute to the peak broadening. If the finite size is not the dominating contributor to peak broadening, the L_c from Scherrer equation is not reflecting the crystallite size but referring to the coherence length of the coherently diffracting regions. A more nuanced interpretation of the peak broadening is required that attempts to disentangle the various contributions to the peak width after careful examination of extrinsic instrumental resolution[63].

Theoretically, the ideal Bragg diffraction from a perfect, infinite crystal would give infinitely sharp peaks with peak width close to zero. In actual X-ray scattering experiments, the diffraction peaks always show peak broadening due to three intrinsic main factors, 1) the finite size of the ordered region, 2) lattice parameter fluctuation, 3) lattice disorder (cumulative disorder). The impact of finite size is conceptually straightforward and analogous to diffraction from a single slit with a reciprocal relation of size and diffraction width. Lattice parameter fluctuation (e_{rms}) is a measure of the variation in *d*-spacings from one ordered region to another[24], as shown in **Figure 1d**, a large scale heterogeneity of the sample. The peak broadening due to the lattice parameter fluctuation is proportional to the order (m) of the diffraction in the form of[65]:

$$\beta_{hkl} = m\frac{e_{rms}}{d_{hkl}} \qquad (1)$$

Where β is the integral breadth (defined as the integral intensity of a peak divided by the maximum intensity/peak height). The lattice disorder can be classified in two forms[24]: i) the noncumulative disorder which is random statistical fluctuations about an ideal lattice position (*e.g.*, due to thermal fluctuations), and ii) the cumulative disorder which produces long-range distortion and prevents long-range order. For cumulative disorder, we will focus on paracrystalline disorder (quantified with g parameter) which is the main contribution of the cumulative disorder. In paracrystalline phase, the distances between atoms in the space lattice are not constant but show correlated statistical fluctuations in both the direction of neighboring atoms and perpendicular to it, preventing long-range order. The peak broadening due to paracrystalline disorder is proportional to the square of order (m^2) of the diffraction in the form of[65]:

$$\beta_{hkl} = \frac{(\pi m g)^2}{d_{hkl}} \qquad (2)$$

Paracrystals follow the empirical α□-law[66], which restricts their size, expressed as:

$$\sqrt{N}\,g = \alpha = 0.15 \pm 0.05 \qquad (3)$$

Where N is the average number of netplane layers with paracrystal size of Nd_{hkl}. Since paracrystallites always have finite size, the paracrystallinity g and finite size both contribute to the peak broadening in a pure paracrystal model. The integral breadth β in angular space is given by[67]:

$$\beta_{hkl} = \frac{1}{d_{hkl}}\left[\frac{1}{N} + (\pi g m)^2\right] \qquad (4)$$

If it is in reciprocal space, there will be a factor of 2πK in the size term like how the Scherrer equation is transferred from angular space to reciprocal space[63].

These different factors impact the diffraction peaks in different ways. The peak width due to the finite size of crystallites is independent of peak order[24]. Noncumulative disorder related to thermal fluctuation, such as Debye-Waller factor, only causes the lowering of the peak intensity with no effect on the peak width and thus will not be discussed extensively. The lattice parameter fluctuation (e_{rms}) results in peak order-dependent (~m) peak broadening and is assumed to lead to Gaussian-shaped peaks (based on the assumption that random variations throughout the measurement follow Gaussian statistics)[24]. In contrast, peak broadening due to paracrystalline disorder is dependent on the square of order (~m^2) while diffraction peaks have a Lorentzian shape[68]. These distinct difference in the characteristic distributions of these three main factors (finite size, g, e_{rms}) to the peak breadth and intensity enables line shape and intensity analysis to disentangle their contributions to the diffraction peaks if multiple peaks are present. In the case where only the first ordered peak is present, definitive assignment can be readily made to paracrystalline disorder if the line shape is predominantly Lorentzian with the assumption of e_{rms} following Gaussian statistics (see **Scheme 1**).

To disentangle the contribution from finite size, g parameter, and e_{rms} to the peak broadening, the presence of higher order peaks (at least three orders) is required. There are three approaches for the shape analysis. The first one is to perform Warren-Averbach (W-A) analysis for comprehensive analysis. The second one is the Williamson-Hall (W-H) analysis to obtain the β-m^2 plot with g from the slope and finite size from the intercept. Additionally, to check whether there is contribution from lattice parameter fluctuation, one can obtain the β-m plot. If it exhibits linear relations, it implies the contribution from lattice parameter fluctuation exists and e_{rms} can be

obtained from the slope according to **equation (1)**. The last one is only for graphical analysis with plotting FWHM/pseudo-Voigt mixing parameter (η) *vs*. diffraction order (m) to determine qualitatively whether there is contribution from lattice parameter fluctuation or paracrystalline disorder as denoted in **Scheme 1**.

In W-A analysis[69, 70], Fourier transform is performed on the diffraction peaks with a Fourier series after careful deconvolution of instrumental resolution, where Fourier coefficients is a product of two terms: the finite size contribution term (independent of peak order), and the disorder (g, e_{rms}) contribution term (dependent of peak order). The Fourier coefficients $A_m(n)$ is in the form of:

$$A_m(n) = A_m^S(n)A_m^D(n) = \frac{< N(n) >}{M}\exp\left[-2\pi^2 m^2\left(n\mathrm{g}^2 + n^2 e_{rms}^2\right)\right] \qquad (5)$$

Where $A_m^S(n)$ and $A_m^D(n)$ are the contribution of finite size and disorder (g, e_{rms}), respectively; n is for Fourier series; m is the diffraction order; $< N(n) >$ is a factor account for column length distribution; and M is the area-weighted column length. Column length refers to crystallite size emphasizing on the length of a column of unit cells stacked along the normal of the diffracting lattice planes (diffraction vector). To perform W-A analysis, first, isolated diffraction peaks need to be obtained with appropriate background subtraction and resolution function correction. Then, there are two approaches: full fit and graphical approach. In the full fit approach, the coefficients of Fourier series are calculated with a fast-Fourier-transform (FFT) algorithm, and then $A_m(n)$ is fitted with **equation (5)** with assumed column length distribution. This fitting will result in the values of column length, g, and e_{rms}, respectively. In the graphical approach[71], first, ln $[A_m(n)]$ *vs*. m^2 is fitted linearly for a constant n, where one obtains values for ln $[\frac{< N(n) >}{M}]$ from the intercept and $f(n) = \mathrm{g}^2 + ne_{rms}^2$ from the slope of each curve with a certain n. Then, another linear fit of $f(n)$ *vs. n* will yield g^2 and e_{rms}^2. In W-A analysis, the information contained in the complete peak shape (width and intensity) is considered via Fourier transform. In contrast, W-H analysis[72] only takes into account of peak width. In practice of semiconducting polymer cases, X. Jiao *et al.*[73] applied W-H method in angular space with the form of:

$$\beta = \beta_S + \beta_D = \frac{1}{< L >_V} + \frac{\pi^2 \mathrm{g}^2}{d} m^2 \qquad (6)$$

Where β is the diffraction peak width corrected for instrumental resolution, β_S and β_D is the contribution of finite size and paracrystalline disorder, $<L>_V$ is the volume-weighted column length. (We note that this reflects **equation (4)** with the same contribution of the *g* parameter.) In reciprocal space, the **equation (6)** is in the form of:

$$\beta = \frac{2\pi K}{<L>_V} + \frac{\pi^2 g^2}{d} m^2 \qquad (7)$$

In W-H analysis, the contribution from lattice parameter fluctuation is not taken into account or ignored. To determine whether there is contribution from lattice parameter fluctuation, the β-*m* plot can be applied. If it shows a linear relation, the contribution from lattice parameter fluctuation exists[65]. In this case, e_{rms} can be obtained from the slope according to the **equation (1)**.

The graphical analysis[24] (option 3 in **Scheme 1**) is to estimate the contribution of finite size, *g*, and e_{rms} only qualitatively, and thus it cannot give the exact values of *g*, or e_{rms}. First, we disentangle the contribution of finite size from disorder which includes both paracrystalline disorder (*g*) and lattice parameter fluctuation (e_{rms}). We plot the peak width (FWHM) as a function of peak orders (*m*). The schematic cases shown in **Figure 2c** illustrate that when the finite size is the only contributor to the broadening of peaks, the peak width is a constant as a function of peak orders[23]. If there is also a contribution from disorder, the peak width shows an increasing trend with peak orders. An experimental example[24] is shown in **Figure 2d,** where the data for TIPS-pentacene, a polycrystalline organic conductor with small lattice disorder, is dominated by finite size effect with a roughly constant peak width, whereas lattice disorder is observed in P(NDI2OD-T2) and PBTTT with linear increasing peak width with peak orders. Then, if the peak broadening is dominated by disorder terms, we can disentangle the contribution from paracrystalline disorder (*g*) and lattice parameter fluctuation (e_{rms}) with the help of pseudo-Voigt mixing parameter η with peak shape analysis, where η is the Lorentzian fraction when a peak is fitted with the Voigt function with a linear combination of Gaussian and Lorentzian. This analysis makes use of the fact that paracrystallinity produces a Lorentzian peak shape[68] while the lattice-parameter fluctuation is assumed to produce a Gaussian shape[24] if it follows Gaussian statistics. η close to 1 (Lorentzian) indicates *g*-dominated disorder while η close to 0 (Gaussian) suggests e_{rms}-dominated disorder. In the cases where η is not close to 0 or 1, both paracrystallinity and lattice parameter fluctuations exist. An example is shown in **Figure 2e.** TIPS-pentacene has an η<0.5 and a decreasing trend

with diffraction order, suggesting highly crystalline behavior with a very low *g*. In contrast, P(NDI2OD-T2) shows a relatively constant $\eta \sim 0.75$, illustrating a competition between paracrystalline disorder and lattice parameter fluctuations. PBTTT with $\eta \sim 1$ shows strong paracrystalline disorder. For $\eta < 0.5$, the width of the peak is dominated by the lattice parameter fluctuations and the possibility of contribution from finite size cannot be excluded. For η close to 1, the peak width is dominated by the coherence length of the cumulative disorder (paracrystallinity).

In summary, all these three approaches require multiple (at least three) diffraction orders, and thus making the application in conjugated polymer cases limited. W-A analysis gives the most comprehensive understanding of the peak broadening with the ability to provide quantitative values of all three contributors (crystallite size, *g*, and e_{rms}). However, it requires high-quality diffraction data. In W-H analysis, the values of coherence length and *g* can be obtained while the contribution of e_{rms} is not taken into account. To obtain e_{rms}, one can use the β-*m* plot. Moreover, the derivation of W-H method assumes the Lorentzian peak broadening, which might not be fulfilled in most cases. The graphical analysis is a qualitative and simplified method to determine the contribution from finite size, *g* parameter, and e_{rms} qualitatively without extracting the exact values.

For the size scale (crystallite size or coherence length) and *g* parameter, the values extracted from Scherrer equation, W-H or W-A analysis do not match with each other in semiconducting polymers. For the size scale, J. Rivnay *et al*.[24] has a thorough discussion. When finite size dominates the peak broadening, L_c from Scherrer equation is a good approximate for the crystallite size, which is comparable to that extracted from W-H and W-A analysis. For example, in (00*l*) peaks of TIPS-Pentacene[24], the L_c from Scherrer equation is 95.2 nm. The volume-weighted column length from W-H analysis is 97.5 nm while the area-weighted column length from W-A analysis is 67-87 nm (depending on the method and size distribution used). Generally, volume-weighted column length is larger than area-weighted column length with a factor of 1-3[74]. In (*h*00) peaks of P3DDT[71], the L_c from Scherrer equation is 15.3 nm while the column length from W-H and W-A analysis is 14.6 nm and 17.1 nm, respectively. If the contributions of size and disorder effects to the peak breadth are comparable, these two contributions need to be decoupled with W-H or W-A analysis. For the accurate determination of disorder terms, the latter is preferred. For example, in (*h*00) peaks of

P(NDI2OD-T2)[24], the L_c from Scherrer equation is 27.8 nm while the column length from W-H and W-A analysis is 34.0 nm and 22-27 nm, respectively. If the disorder effects dominate the peak broadening, the crystallite size cannot be determined from diffraction line-shape analysis. L_c from Scherrer equation reflects the coherence length of the domains that diffracted coherently. For the *g* parameter, W-A analysis gives the most accurate values while W-H analysis tends to get overestimated since it ignores the possible contribution from lattice parameter fluctuation. The *g* parameters from W-H and W-A analysis are 2.15% *vs.* 0.3-0.84% for (00*l*) peaks of TIPS-Pentacene, 10% *vs.* 1.6% for (*h*00) peaks of P3DDT, and 9.2% *vs.* 3.6-4.6% for (*h*00) peaks of P(NDI2OD-T2).

In most cases, only the first order peaks (*e.g.*, (100) and (010)) are observed. Neither W-A analysis nor W-H analysis can be performed. However, *g* parameter determination is essential in the classification scheme in Section 3 and likely important for its relation to opto-electronic properties. To estimate the *g* parameter, it has become common practice to use a single peak estimation with $g \approx \frac{1}{2\pi}\sqrt{\Delta q \cdot d_{hkl}}$ on the condition that $\eta \sim 1$, where Δq and d_{hkl} are the FWHM and the interplanar spacing of the diffraction peak of interest. Such *g* parameter estimation is intended to assure that the contribution from lattice parameter fluctuation is small with the condition $\eta \sim 1$ since paracrystallinity leads to Lorentzian peak ($\eta = 1$) while lattice parameter fluctuation is assumed to result in Gaussian peak ($\eta = 0$). It is also assumed that finite size contributions can be ignored[24]. Although this method is oversimplified and the assumptions are likely not always fulfilled, it is widely used as the only accessible interpretation when only first order peaks are present. This is especially the case for (0*k*0) peaks where only the first order diffraction is present while π-π stacking properties is important since it is thought to be more relevant to performance than lamellar stacking. With $\eta \sim 1$ (negligible contribution from e_{rms}), this single peak estimation can be a good estimate of *g* parameter. For example, PBTTT shows strong paracrystalline disorder with $\eta \sim 1$, and thus the *g* parameter of (0*k*0) from W-A analysis (~7.3%)[24] and from the single-peak analysis (8%) are close to each other. However, when effects from Gaussian lattice parameter fluctuations are comparable to or even greater than paracrystalline disorder, the single-peak analysis is not applicable. For example, the *g* parameter for P(NDI2OD-T2) (*h*00) peaks and TIPS-pentacene (00*l*) peaks from the single-peak analysis are 14%, 5% respectively, which are not consistent with results from W-A analysis (4%, 0.3%)[24].

For many of the polymers discussed in the next section, paracrystalline disorder dominates the (010) peaks with η close to 1, such as PTQ10 (~1), PBDB-T (~1), P(NDI2OD-T2) (~1), PffBT4T-2OD (~0.96), PTB7-Th (~0.94) and DPP3T (~0.80), and thus the single-peak estimation is applicable with the assumptions stated above. In contrast, paracrystalline disorder is not dominating the (h00) peaks in many cases, such as PTQ10, PM6, and DPP3T (as shown in **Figure 5n**). In these cases, the single-peak estimation for g parameter determination cannot be performed. Since there show three diffraction orders, the W-H analysis is applicable. Generally, g = 0% indicates a perfect crystal and 0% < g < 2% represents crystalline ordering, while 2% < g < 12% is considered to correspond to paracrystalline ordering; Amorphous silicon dioxide glass has $g \approx$ 12% and thus materials with g >12% have generally been referred to be amorphous when considering X-ray analysis alone. The g parameter is thus an important metric when trying to classify semiconducting polymers.

Determination of DoC

In X-ray diffraction experiments, the integrated intensity of the diffraction peaks associated with the ordered volume fraction is often proportional to the amount of crystalline/ordered material in a thin film with fiber texture[23], and thus can quantify the relative DoC. However, an absolute DoC is close to impossible to be quantified since it would require reference samples to be entirely crystalline or entirely amorphous, which is hardly obtained in polymeric materials. Instead, the relative DoC (rDoC)[23, 75, 76], describing the DoC of one film as compared to another film of the same material and film thickness, can be quantified. Generally, the rDoC can be quantified by several methods, such as GIWAXS, DSC, NMR, and density via dilatometer. There are mainly two different ways to characterize the rDoC via GIWAXS. The first method that quantifies the DoC relies on analyzing and quantitatively separating the scattering intensity originated from amorphous domains with that from ordered domains[77-79]. J. Balko *et al.*[79] proposed that the DoC can be estimated from the percentage of amorphous domains evaluated by the ratio of the intensity at a certain scattering angle between (100) and (200) peaks in the semicrystalline sample to that in a completely amorphous (molten) sample. The second and mostly used method only gives rDoC, which is to integrate the intensity of an Ewald sphere corrected, complete pole figure from out-of-plane direction to in-plane direction. This integrated intensity is proportional to a film's DoC[59] for

fiber texture. When comparing the integrated intensity between samples with the sample material but different processing conditions, the rDoC can be extracted.

The possibility for NMR to determine DoC arises through an intrinsic difference between the nuclear resonance frequency of the targeted nuclei, such as ^{1}H and ^{13}C, of the ordered domains and the amorphous domains. After decomposition of the resonance spectra into the two parts of ordered and amorphous components, the DoC is given by the percentage of the intensity of the ordered components[75, 80]. DSC is an absolute method. In the DSC method, the DoC is characterized by the ratio of the specific enthalpy of fusion of the semicrystalline material to that of a 100% crystalline material[79]. However, pure crystalline materials are not available for most polymers. The reference melting enthalpy of a 100% crystalline material needs to be corrected for finite crystal size[76] or extrapolated with the help of GIWAXS or NMR data[79]. rDoC can also be characterized by measuring the mass density with density gradient column[75]. The measured mass density of a semicrystalline material is assumed to be the sum of the percentage of the mass density of the crystalline and amorphous components. The mass density of the amorphous components can be estimated from the molten state[81] and that of a 100% crystalline material can be calculated based on the structural information of the unit cell[82]. It should be noted that various methods described above do not necessarily give the same values of DoC since the detected order or crystallinity depends on the sensitivity of the techniques. For example, DoC determined by NMR is often greater than that from X-ray diffraction since NMR peaks of ordered phases are based on the segmental conformation. Local order can contribute to NMR peak, but not for X-ray diffraction peaks. However, DoC values from different methods are in qualitative and relative agreement with each other. For example, rr-P3HT with molecular weight of 13 kg/mol, 23 kg/mol, 34 kg/mol are reported with DoC of 56%, 49%, 47% from X-ray diffraction, 66%, 60%, 56% from NMR, and 41%, 22%, 17% from mass density, respectively[75].

Characteristic length versus size and associated terminology

An important issue for any GIWAXS measurements is what kind of length scale is determined and how it is translated into a size. There are often two different size scales in a material that need to be differentiated conceptually. A domain may consist of several grains or crystallites which are fused together with large or small angle grain boundaries[83, 84] (**Figure 3a**). In the literature, domain and grain are often used incorrectly interchangeably, yet it is grain and crystallites that are

synonymous. To avoid confusion and provide consistency, we follow the terminology of the Salleo group[23, 83, 85]. Furthermore, grain is the terminology of inorganic materials or small molecule systems. For semiconducting polymers, crystallite is used almost universally and we simply have only ordered domains with domains walls or disordered material between crystallites. As the quality of the ordering decreases and the paracrystallinity increases, what is determined by X-ray analysis is strictly speaking no longer the size of a crystallite, but column length that gives rise to coherent scattering. Since **equation (3)** asserts empirically that real paracrystallites have finite size, one can, in practical terms, think of the materials consisting now of paracrystallites which are defined by their size determined by **equation (3)** if the *g* parameter is obtained. We caution though that such conversion to size should be taken with a grain of salt, as Scherer equation, W-H, W-A, and α-law are not consistent with each other. Relative comparison using the same analysis protocols to differentiate changes between samples will be safest when drawing conclusions.

The domain size and shape are generally not accessible by GIWAXS, but by light microscopy, atomic force microscope (AFM), polarized optical microscopy (POM), scanning tunneling microscopy (STM), or small angle X-ray scattering (SAXS) or resonant soft X-ray scattering (RSoXS). Crystallite size is accessible with GIWAXS if the defects inside the crystallite do not affect the coherent diffracting. In general, the spatial extent that is measured in GIWAXS is the characteristic length of coherently diffracting regions[71]. The interpretation of the resulting coherence length is subject to the analysis described above and summarized in **Scheme 1**. To unambiguously determine size, W-A analysis is required. Size cannot be unambiguously assessed with GIWAXS from a single peak.

This kind of size relation on multiple length scales exists even in domains referred as “single crystals”. For example, macroscopic single crystals of polyethylene (PE) exhibit a well-defined rhombus shape, but are actually composed of many so-called micro-paracrystals (MPC)[66], as shown in **Figure 4b**. In order to be consistent with the commonly used crystallite terminology, we call the MPCs paracrystallites. Similarly, in semiconducting polymer cases of P3HT, STM images show clear domains composed of fused grains or crystallites spanning over hundreds of nanometers (**Figure 4c)**, where the crystallites with different orientations are interconnected by folded chains. Even PM6 shows similar size relation. The AFM phase image of PM6[86] (**Figure 4d)** implies ordered regions embedded in a disordered matrix with the ordered regions tens of

nanometers in size, while the coherence length of (100) and (010) are only 7.4 nm, and 4.9 nm, respectively from Scherrer analysis of the GIWAXS data (**Table 1**). The size from **equation (3)** would be 1.4 nm for (100) and 0.27 nm for (010), pointing out again the discrepancy.

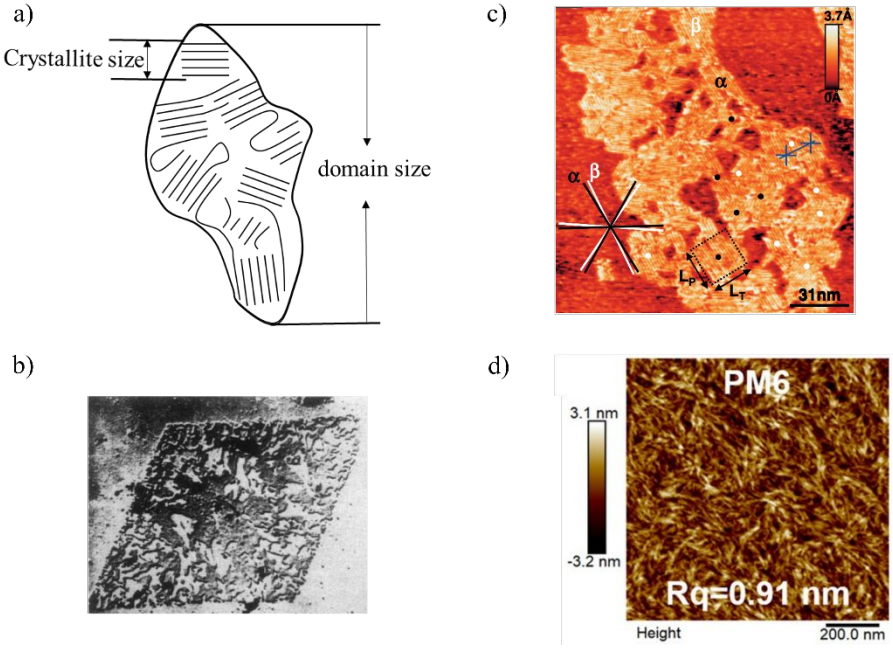

Figure 3. a) Schematics for a domain composed of crystallites. b) TEM image of the 'single crystal' of polyethylene, indicating that it actually consists of 300Å MPCs aligned parallel to each other[66]. Adapted with permission from ref. 66. c) 153.7 nm × 157.1 nm scanning tunneling microscopy (STM) image of P3HT[84]. Adapted with permission from ref. 84. d) The AFM phase image for neat PM6[86]. Adapted with permission from ref. 86.

Blends

In many applications, such as OSC blends, the diffraction peaks of the two or more components often overlap, particularly the (010) peaks, and quantitative GIWAXS analysis is considerably complicated if not entirely prevented. This complication has in part hampered achieving universal insight regarding the desirability of the degree of ordering and quality of ordering in OSCs as well as other applications using blends. We note, as will be shown explicitly below, that many of the best donor polymers for OSC applications (*e.g.*, FTAZ, PTB7-Th, and PM6) are not very well ordered. Nonetheless, positive correlations in performance are generally associated with improved

molecular ordering (*i.e.*, larger coherence length and higher DoC/DoO) as well as face-on orientation[87, 88]. This complex applied topic warrants its own review.

3. Classification of Ordering According to Melting and the *g* Parameters

In this section, we are going to delineate five broad classification categories based on the degree of disorder (amorphous to semi-paracrystalline) and provide some examples of a broad range of representative polymers as illustrations and examples with the materials shown in **Figure 4**. For the semi-paracrystalline materials, we will only discuss the paracrystalline portions. The GIWAXS data and shape analysis results for (*h*00) peaks (to determine whether single peak estimation of *g* is applicable) along with the DSC thermograms are shown in **Figure 5**. Key parameters derived from GIWAXS and DSC for classification are summarized in **Table 1** and **Figure 6**. All GIWAXS data are acquired at beamline 7.3.3 at Advance Light Source (ALS)[89]. The FWHMs used for L_c and *g* estimation in **Table 1** have been corrected from instrumental resolution including the contributions from the beam divergence, the beam bandwidth and the geometric smearing[63].

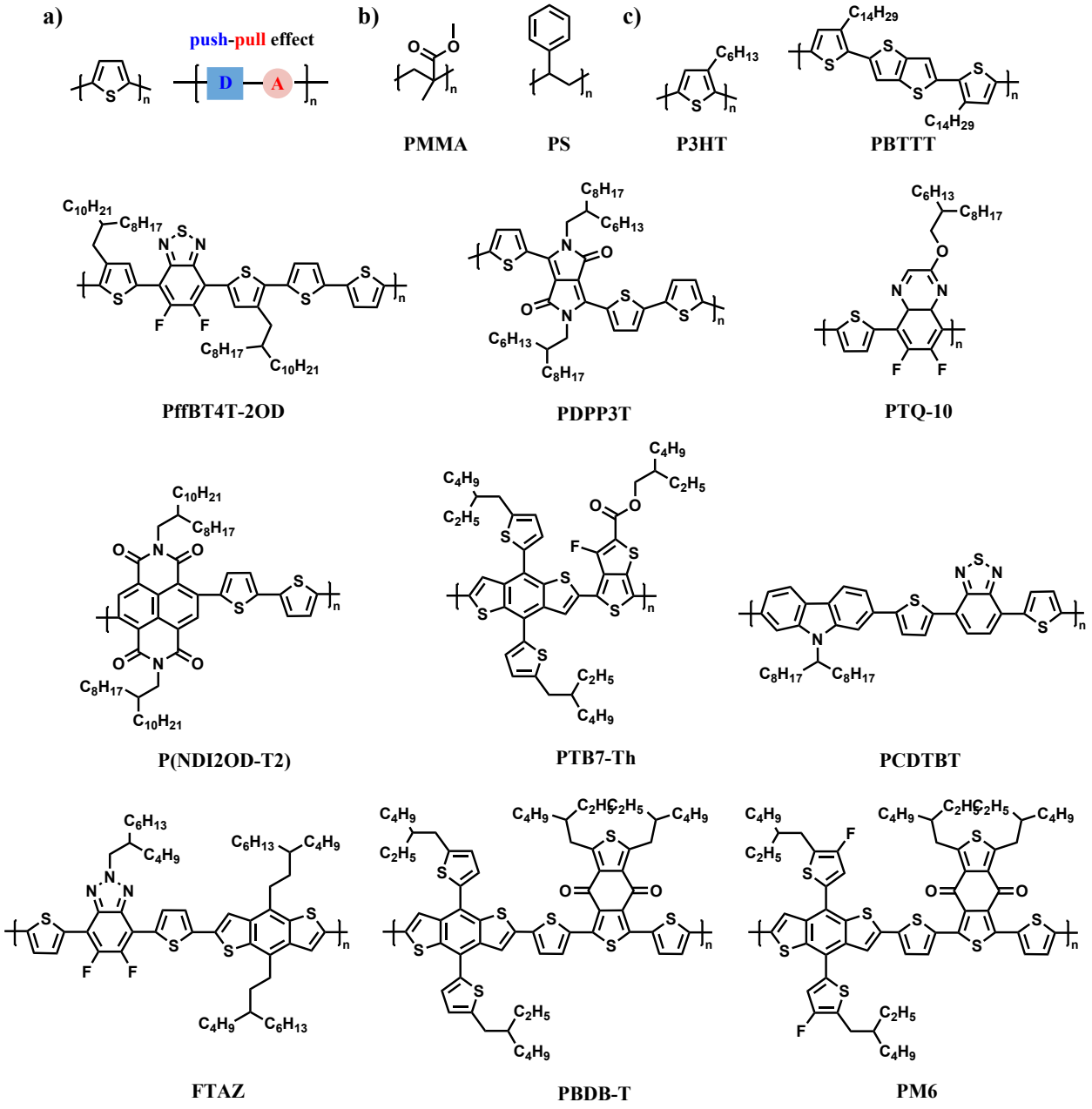

Figure 4. a) Two types of conjugated polymers (left: homopolymers, which may have various sidechains, right: donor-acceptor (D-A) alternating conjugated copolymers with push-pull effect). b) The chemical structure of two amorphous nonconjugated reference polymers. c) The chemical structure of the conjugated polymers used here.

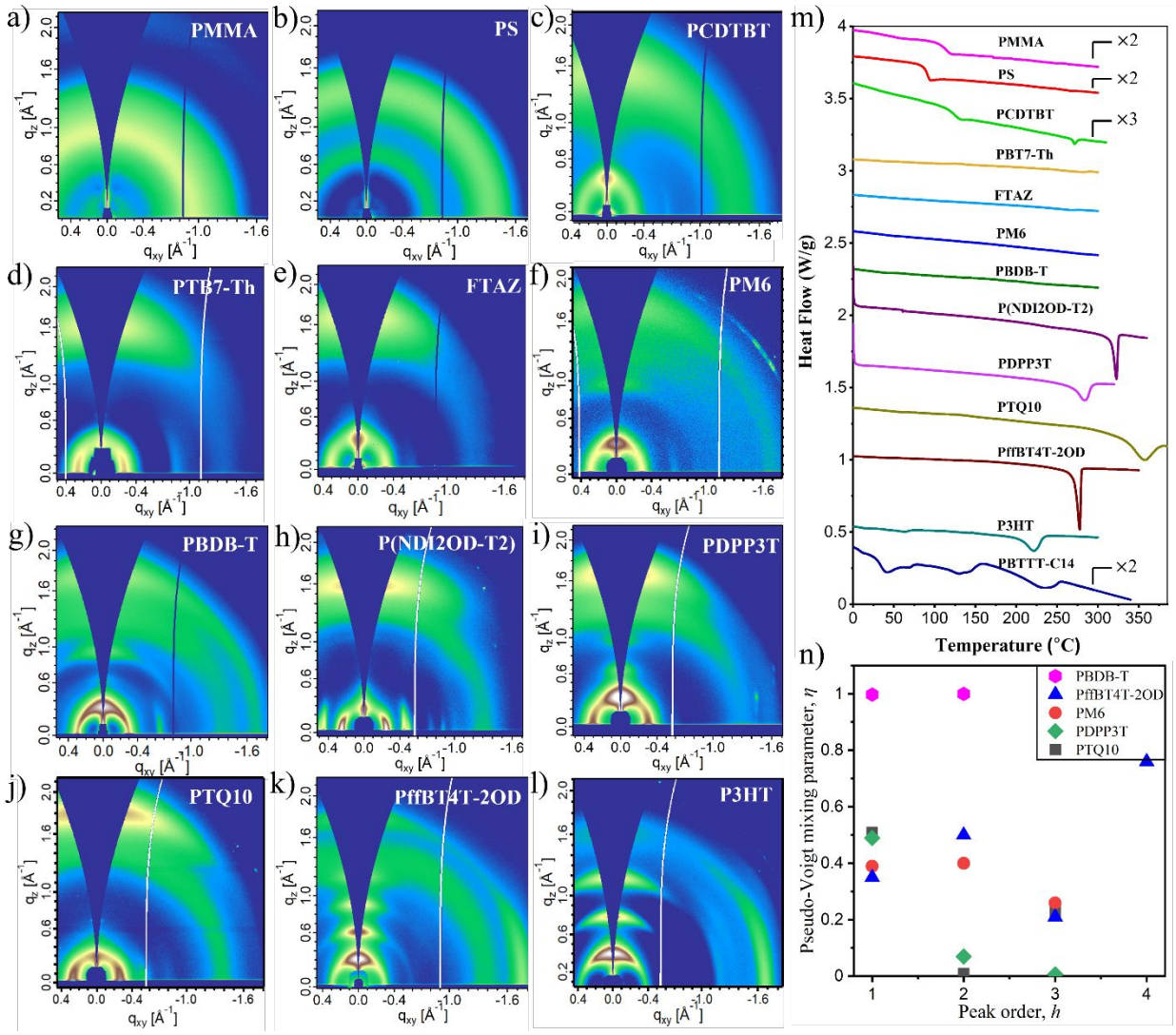

Figure 5. a-l) The GIWAXS patterns of PMMA, PS, PCDTBT, PTB7-Th, FTAZ, PM6, PBDB-T, P(NDI2OD-T2), DPP3T, PTQ10, PffBT4T-2OD, and PBTTT-C12, respectively. m) The 1st heating of DSC thermograms with the heating rate of 10 ℃/min of neat materials solution-cast from chlorobenzene (expect for PMMA, PS, PM6, PCDTBT, and PTQ10 which are cast from chloroform). Since the highest temperature reached here is ~ 300 ― 390 ℃, we cannot rule out the possibility of features (*e.g.*, melting peak) beyond the measured range. The thermograms were vertically shifted and some profiles are enlarged to magnify the features. n) Pseudo-Voigt mixing parameter, η, as a function of peak order of (h00).

Table 1. Summary of parameters characterized by DSC and GIWAXS for representative conjugated polymers of high interest in organic electronics. Two amorphous insulating polymers (PS and PMMA) and crystalline TIPS pentacene are included for comparison purposes.

Polymer	Melting temperature T_m (ΔT[a]) [℃]	Melting enthalpy ΔH_m [J/g]	Highest (h00) order (h)	L_c of lamellar stacking ($L_{c\,(100)}$) [nm]	Number of (100) stacked layers	L_c of π-stacking ($L_{c\,(010)}$) [nm]	Number of π-stacked layers (n)	η *of* (100)/(010)	g for (100) peak	g for (010) peak	Remark
PMMA	N/A	N/A	N/A	N/A	N/A	1.4	2.1	/0.99	N/A	28%[b]	3D amorphous
PS	N/A	N/A	N/A	N/A	N/A	1.3	2.7	/0.8	N/A	24%[b]	3D amorphous
PCDTBT	271.5 (10.5)	1.14	1	> 2.7[c]	1.5	1.6	4.2	0.32/1	32%[90]	20%	Oriented amorphous
PTB7-Th	N/A	N/A	1	5.3	2.3	1.5	3.8	0.6/0.94	27%	20%	Highly disordered
FTAZ	N/A	N/A	1	5.8	2.9	1.7	4.6	0.55/1	-	19%	Highly disordered
PBDB-T	N/A	N/A	3	10.8	5.1	1.9	5.1	1/1	14%	18%	Highly disordered
PM6	N/A	N/A	3	7.9	4.2	1.8	4.9	0.6/0.6	17%	18%	Highly disordered
P(NDI2OD-T2)	312.3 (12.0)	15.9	4	> 44.3[c]	17.8	1.6	5.7	0.4/1	4%[24]	17%	2D semi-paracrystalline
PDPP3T	283.5 (27.1)	17.4	3	> 7.4[c]	3.9	2.0	5.3	0.35/0.8	13%	17%	2D semi-paracrystalline
PTQ10	356.7 (47.3)	17.7	3	> 9.7[c]	4.2	3.4	9.8	0.5/1	13%	13%	2D semi-paracrystalline
PffBT4T-2OD	277.8 (8.9)	21.5	4	> 22.1[c]	10.9	5.1	14.7	0.35/0.96	10%	11%	3D semi-paracrystalline
P3HT	222.8 (18.3)	19.7	3	15.7	9.2	7.0	18.4	0.25/1	8%	9%	3D semi-paracrystalline
PBTTT	230.8 (60.6)	23.2	4[91]	15.7	7.9	8.3[91]	22.3	-/1	7%[91]	8%	3D semi-paracrystalline
TIPS-Pentacene	261 (4.3)[92]	25.6[92]	4[24]	-	-	89.7[93]	115.0	-	0.3%[24]	4%[24]	Crystalline

Here, the g parameter for (100) of PBDB-T, PM6, DPP3T, PTQ10, PffBT4T-2OD, and P3HT are obtained from the W-H analysis while all other g parameters are estimated with single-peak width analysis, which is a good estimation of the paracrystallinity when paracrystallinity dominates the peak shape[24]. N/A refers to that the materials do not show corresponding features. "-" refers to that the corresponding parameters are able to be extracted for the materials, but we do not have the data here.

[a] ΔT refers to the peak width of the melting peak.

[b] Since there is no π-π stacking peak for PS and PMMA, the peak used here is their amorphous peak with the highest intensity.

[c] " > " is due to the $\eta < 0.5$, which implies that lattice parameter fluctuation and/or finite size contribute to the peak broadening. If lattice parameter fluctuation dominates the peak broadening, we cannot make any conclusion on size scale. Here we take the values from the Scherrer equation as a lower limit. Given the higher (h00) orders observed, PM6 and PBDB-T might be 2D para-crystalline with a T_m that is not detectable in DSC. TIPS-Pentacene is not a polymer, but a crystalline organic semiconductor that is included here as a reference for material considered highly crystalline despite a $g_{(010)}$ of 4%. The data of the 10th column for TIPS-Pentacene is shown for (001) stacking.

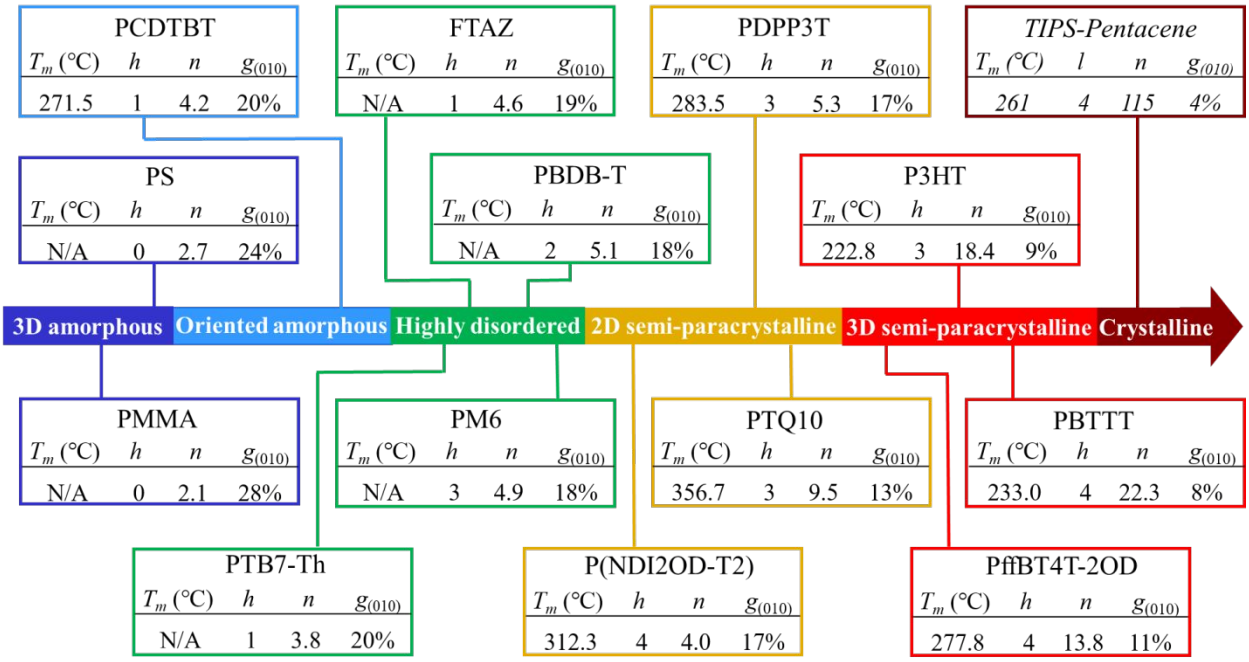

Figure 6. Summary of 11 representative semiconducting polymers on a disorder-order scale characterized by the *g* parameter of the (010) peak. Relevant parameters such as T_m, *h* (*l*), *n*, and $g_{(010)}$ refer to the melting temperature (in Celsius), the presence of the highest order of lamellar (backbone) stacking, the number of π-π stacked layers, and the paracrystalline disorder parameter for (010) peaks, respectively. We note that TIPS-Pentacene is not a polymer, but an organic small molecule semiconductor typically considered "crystalline".

The 2D patterns shown in **Figure 5** do not exhibit off-axis, mixed index peaks (*hkl*) and there is not enough ordering and information for unit cell parameters determination. It is assumed that the molecular packing is orthorhombic unless explicitly noted. Furthermore, the molecular ordering

of a material depends on its processing history (casting solvents, additives, annealing, coating method, *etc*.). To provide some aspects of relative comparison, all GIWAXS data provided in **Figure 5** are acquired from as-cast films spin-cast with chlorobenzene and without any additive, and the DSC data are acquired at a rate of 10 ℃/min heating/cooling from films drop-cast from chlorobenzene. The presence/absence of melting peak in DSC is a critical feature for the classification of amorphous/highly disordered or semi-paracrystalline that will be discussed in detail below. However, the highest temperature reached here is ~ 300 – 390 ℃ (**Figure 5** m), we cannot rule out the possibility of the presence of melting peak beyond the measured range. The classification below for specific polymers will be only based on the data we have. The properties of the molecular ordering characterized here are processing dependent rather than the intrinsic properties of the polymers at the thermodynamic limit.

Combining GIWAXS and DSC, we classify the polymers as described below into categories, based on the degree of disorder and the presence or absence of a glass transition or melting transition: 3D amorphous, oriented amorphous, highly disordered, 2D semi-paracrystalline (2D paracrystallites) with g < 12% along the most ordered direction but amorphous/highly paracrystalline characteristics along the least ordered direction (g > 12%); and 3D semi-paracrystalline (3D paracrystallites) with $g_{(100)}$ < 12% and $g_{(010)}$ < 12%. The labels "crystalline" and "semicrystalline" are reserved for materials with long-range order with g < 2% and DoC of > 80% and < 80%[94], respectively. One key dividing line between amorphous/highly disordered and semi-paracrystalline is the presence or absence of a melting transition in DSC. Samples that show a melting peak in DSC are clearly not amorphous since they possess sufficient ordering in at least one dimension to provide a melting endotherm. We note that based on the melting enthalpies observed here in P3HT (ΔH_m = 19.7 J/g corresponds to DoC of 40% with $\Delta H_m^{\infty}(P3HT) = 49 \pm 2$ J/g[76]), we surmise that even the 3D semi-paracrystalline samples still have a considerable volume fraction of disorder. Hence the use of "semi-" refers to the degree of ordering that is likely less than 50% in most samples. The main difference between 3D amorphous and oriented amorphous/highly disordered samples lies on that 3D amorphous samples show isotropic orientation in GIWAXS peaks while oriented amorphous/highly ordered samples show a certain preferential orientation in GIWAXS peaks. The overall classification scheme is illustrated and displayed in **Figure 7** and quantitative analysis results are summarized in **Table 2**. Care must be exercised with criterion as only a θ-2θ scan or rocking scan will provide accurate intensities along

the specular rods (h00). In GIWAXS, the extent of the arching of the (h00) peaks needs to be considered as the visibility of higher orders is strongly coupled to mosaicity where a highly ordered film with very small mosaicity (near perfect edge-on orientation) might only show a first order peak along (h00)[95]. We will discuss these classes and their defining characteristics in turn using a number of representative materials.

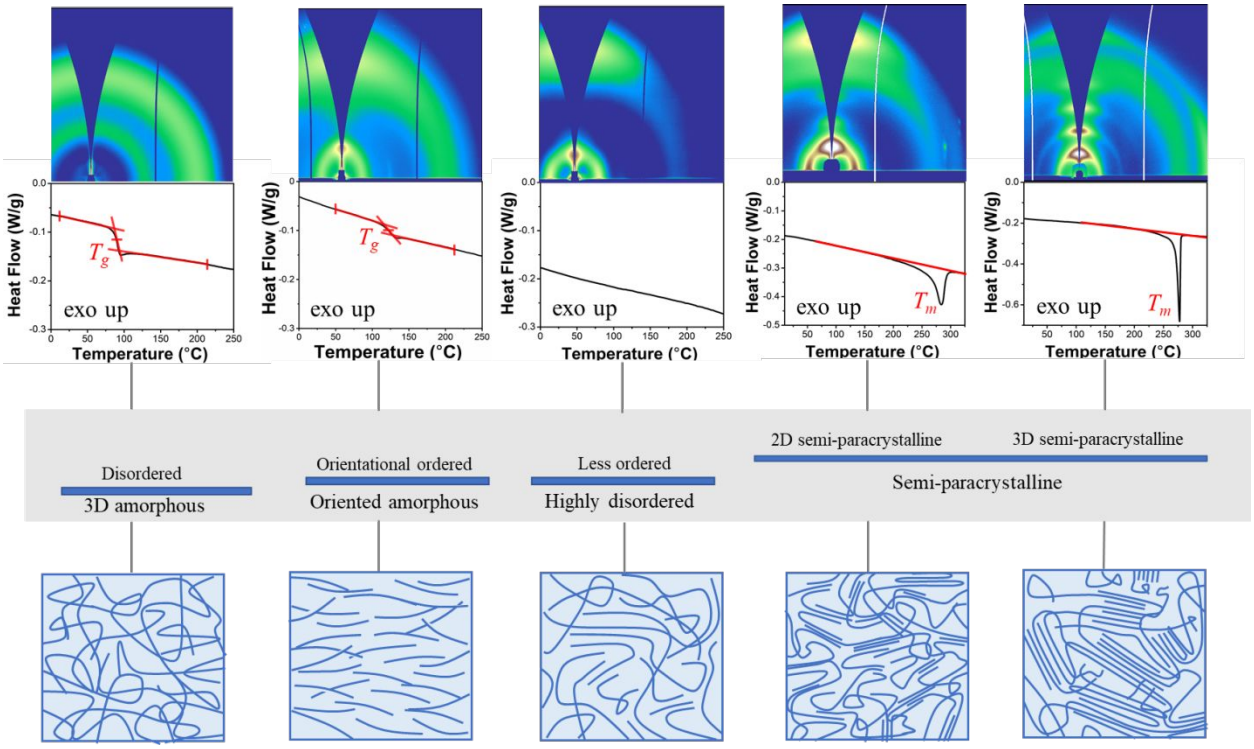

Figure 7. Qualitative classification of molecular ordering of a polymer material on the quantitative order-disorder scale using both GIWAXS and DSC criteria and schematic representations for various ordering. The 3D amorphous materials show glass transition and no melting peak in DSC and broad, featureless, isotropic scattering peaks in the GIWAXS pattern. The oriented amorphous/highly disordered conjugated polymers only show lowest order, broad peaks in the GIWAXS pattern (indicating some local short-range orientational order) with no melting peak in DSC heating scan while oriented amorphous polymers show a T_g in DSC but highly disordered polymers do not. The ordered (semi-paracrystalline) material can be characterized by a melting peak observed in DSC and 2D or 3D ordering according to the GIWAXS data and g parameter analysis. For the ordered conjugated polymers, we classify them into two types, the 2D and 3D semi-paracrystalline. Both classes show a melting transition in DSC, although with different widths, and the GIWAXS yields different g parameters. Note that the baselines in the DSC traces are highlighted with red lines to help characterize the thermal transitions.

Table 2. Summary of classification criteria for semiconducting polymers

Classification	T_g observed in DSC	T_m observed in DSC	Highest (h00) order	Highest number of stacked layers	g for the least ordered peak	g for the most ordered peak
3D amorphous	Yes	No	1	1-3	$\geq 12\%$	$\geq 12\%$
Oriented amorphous	Yes	No	1	1-3	$\geq 12\%$	$\geq 12\%$
Highly disordered	No	No	1-3	3-5	$\geq 12\%$	$\geq 12\%$
2D semi-paracrystalline (2D paracrystallite)	No	Yes	≥ 3	≥ 5	$\geq 12\%$	$< 12\%$
3D semi-paracrystalline (3D paracrystallite)	No	Yes	≥ 3	≥ 10	2-12%	2-12%
Crystalline (crystallite)	No	Yes	≥ 3	≥ 10	$\leq 2\%$	$\leq 2\%$

For 3D amorphous polymers, we start the discussion with a pair of classical, amorphous polymers, atactic PS and PMMA, and then extend to representative 3D amorphous conjugated polymers. The GIWAXS patterns for atactic PS and PMMA are depicted in **Figure 5**. Although the atactic PS and PMMA are commonly identified to be amorphous polymers, they still scatter diffusely in GIWAXS experiments and show some scattering peaks. However, these scattering peaks are all broad and isotropically orientated in all angles, which is reported to be the halo patterns of amorphous polymers[96], indicating the disordered/amorphous or noncrystalline state as well as the random texture. Atactic PS shows two scattering peaks at q ~0.71 Å^{-1} and ~1.36 Å^{-1}, corresponding to an average spacing of 8.8 Å and 4.6 Å, respectively. After careful multi-peak fitting with Voigt distribution and a log cubic background, the fitted FWHM of the two peaks are 0.48 Å^{-1} and 0.5 Å^{-1}, respectively, corresponding to a L_c of 1.31 nm and 1.26 nm. Since the peaks are so broad, it is difficult to differentiate the background intensity from the tail of a broad peak, the peak widths fitting here have relatively large uncertainty. Comparing the L_c values (1.31 nm and 1.26 nm) with nominal d-spacings (8.8 Å and 4.6 Å), the L_c is only around two to three molecular layers thick, which is similar to that of a disordered liquid, indicating the disordered properties of PS. The g parameter estimated from single-peak analysis of the peaks at ~0.71 Å^{-1} and ~1.36 Å^{-1} of atactic PS is calculated to be 32.8% and 24.2%, respectively. It is current practice that $g = 12\%$, which

is the *g* parameter of the amorphous glassy materials such as amorphous SiO_x/Si,[97] marks the boundary of amorphous and semicrystalline. The high *g* parameter in atactic PS suggests that it is indeed amorphous and even more disordered than amorphous SiO_x. PMMA also shows a similarly broad, isotropically orientated scattering peak that corresponds to approximately two molecular layers for the peak located at ~ 0.96 $Å^{-1}$. The *g* parameter is estimated to be 28%, again indicating an amorphous material. Meanwhile, the DSC thermograms of atactic PS and PMMA show no melting peak, but a pronounced glass transition, confirming that atactic PS and PMMA are amorphous polymer with their properties summarized in **Table 1**. Some non-polymeric examples of amorphous materials are supercooled liquids and molecular glasses[98, 99], like *o*-terphenyl. For conjugated polymers, materials such as regio-random P3HT and PTAA[27] are 3D amorphous polymers, with a broad, featureless scattering peak in GIWAXS. With regard to nomenclature, 3D amorphous polymers are fully amorphous with the lack of positional ordering in any direction. The examples of PS and PMMA illustrate nicely that observation of a diffraction/scattering peak does not indicate "ordering", much less any degree of "crystallinity", a fact worth keeping in mind when qualitatively describing and analyzing GIWAXS data of semiconducting polymers.

For highly disordered conjugated polymers, there is no observable melting peak in DSC. In addition, their GIWAXS patterns generally only exhibit a (100) lamellar peak and a (010) π-π stacking peak, without any higher order (*h*00) peaks. We call it "highly disordered" rather than "amorphous" since there is no observable glass transition in conventional DSC, which is reported to be ascribed to the stiff backbone that yields a minimal conformation change above and below T_g with a small specific heat capacity change[100]. Take PTB7-Th as an example, there is no melting peak observed in the DSC scan, neither clear glass transition due to the increased conjugation in backbone with large aromatic rings. With GIWAXS, PTB7-Th only shows the alkyl lamellar peak (100) at ~ 0.27 $Å^{-1}$ and π-π stacking peak (010) at ~1.61 $Å^{-1}$, as shown in **Figure 5**. The L_c of (100) and (010) peak is 5.3 nm and 1.5 nm, respectively, which corresponds to around 2.3 and 3.8 molecular layers in the lamellar and π-π stacking direction, respectively (details in **Table 1**), suggesting that the stacking in this direction is not extensive with only some local short-range orientational order. The *g* parameter related to the (100) and (010) peak is around 27% and 20%, implying amorphous characteristic in this direction. Some other important and popular polymers such as FTAZ, PBDB-T, and PM6 (for details see **Table 1)** show similar GIWAXS and DSC characteristics, such as disordered (100) and (010) peaks with corresponding *g* parameters >12%,

absence of the higher order diffraction peaks, and absence of melting peak in DSC scans. We note that PBDB-T and PM6 might be exceptions, in that they do exhibit higher order (*h*00) peaks. The pseudo-Voigt mixing parameter η of (*h*00) and (010) for PBDB-T is ~1, indicating paracrystallinity dominates peak broadening, with *g* parameters of 19% and 18%, respectively. This strong disorder (only 3-5 layers of lamellar and π-π stacking) might explain the lack of melting peak in DSC. However, we cannot rule out the possibility that some of the polymers classified here as highly disordered might be locally ordered enough that more sensitive techniques, such as fast scanning calorimetry (or so-called flash DSC), might be able to detect melting. We emphasize here that the ordering or packing is so limited in range (to 2-5 molecules) in all directions that we advocate shunning the use of "paracrystallite", let alone "crystallite", as the qualitative label to describe the spatial extent and arrangements of the packing in this category of films and materials.

PCDTBT will be classified as oriented amorphous based on the disorder observed in GIWAXS and the clear T_g observed in DSC. However, it is reported[45] to show some liquid crystalline properties, as we mentioned before. The GIWAXS of neat PCDTBT films as processed by us shows only the first order of alkyl stacking peak (100) at ~ 0.35 $Å^{-1}$ and π-π stacking peak (010) at ~1.65 $Å^{-1}$ in the out-of-plane direction. The peak shape analysis performed at (100) and (010) peaks indicates that the L_c of (100) and (010) peak is 2.7 nm and 1.6 nm, respectively, which is around 1.5 and 4.2 molecular layers, and the corresponding *g* parameter is around 32% and 20%, respectively (see **Table 1**), suggesting that PCDTBT is highly disordered. However, the DSC thermogram scan of PCDTBT shows a small melting peak at 271.5 ℃ with a very small enthalpy of 1.14 J/g, which is consistent with the reported nematic-isotropic transition temperature[45]. The small melting peak in DSC suggests that PCDTBT can be ordered although GIWAXS analysis would classify it as highly disordered. The volume fraction of the nematic-isotropic phase is likely very small as the DSC also shows a very clear T_g transition for PCDTBT from the amorphous phase that is dominating the GIWAXS signature. It is thus the combination of DSC and WAXS that provides for complete classification.

For the semi-paracrystalline conjugated polymers, we classify them into two types, the 2D and 3D semi-paracrystalline. Both classes show a melting transition in DSC, although with different widths, while the GIWAXS yields different *g* parameters. A representative 3D semi-paracrystalline conjugated polymer is P3HT. Its GIWAXS 2D pattern[101] shows distinctive (100),

(200), (300) lamellar peaks observed in the out-of-plane direction with q values of ca. 0.37 Å^{-1}, 0.77 Å^{-1}, 1.14 Å^{-1}, and well-defined π-π stacking peak (010) in the in-plane direction at q ~1.68 Å^{-1}, corresponding a d-spacing of ~3.8 Å. The presence of the higher order (h00) peaks implies better molecular packing of the alkyl chains and better ordering properties than the previously discussed amorphous/highly disordered polymers. Although there is no observed off-axis (*hkl*) peaks for exact unit cell determination with P3HT films processed here (spin cast from chlorobenzene), it is reported in literature for some highly oriented P3HT films. M. Brinkmann *et al.*[82, 102] reported that the highly oriented P3HT thin film via directional epitaxial crystallization show a monoclinic unit cell after detailed analysis with the presence of enough off-axis, mixed (*hkl*) peaks in electron diffraction patterns while T. Prosa *et al.* [103] reported an orthorhombic unit cell for stretch-oriented P3HT films. The L_c of the P3HT (010) peak is 7.0 nm, which is around 18.4 molecular layers in the π-π stacking direction, exhibiting a relatively long-range order in this direction. The g parameter for (010) peak is around 9%, indicating paracrystalline ordering. The DSC scan with a heating rate of 10 ℃/min shows a pronounced melting peak at ~222.8 ℃ with a relatively large melting enthalpy of 19.7 J/g. We label P3HT as 3D semi-paracrystalline based on these DSC and GIWAXS characteristics, *i.e.*, relatively long-range ordered π-π stacking, the presence of higher order (h00) peaks, and the observed melting signal in DSC. Similarly, polymers such as PffBT4T-2OD and PBTTT are also characterized to be 3D semi-paracrystalline. Details are provided in **Table 1**. Only in these cases would it be appropriate to use the qualitative label "3D paracrystallite" to describe the spatial arrangement and extent of the molecular packing.

2D semi-paracrystalline polymers also exhibit a DSC melting peak. In contrast to 3D semi-paracrystalline polymers, there is an apparent lack of ordering in the π-stacking direction as characterized with GIWAXS. Despite the lower ordering in their π-stacks, they can form 2D paracrystallite with local short-range order, providing effective pathways for intermolecular charge transport that results in much higher charge mobility than observed in amorphous/highly disordered polymer systems. A typical 2D semi-paracrystalline conjugated polymer is PDPP3T. The GIWAXS pattern of PDPP3T shows discernible (100), (200), (300) lamellar peaks at q values of around 0.33 Å^{-1}, 0.65 Å^{-1}, 0.95 Å^{-1}, respectively, and (010) π-π stacking peak in the out-of-plane direction at q ~1.66 Å^{-1}, corresponding a d-spacing of ~3.7 Å. The L_c of (010) peak is around 2.03 nm, which is approximately 5.3 molecular layers in the π-π stacking, implying a relatively short-range order in this direction. Moreover, the g parameter for (010) peak is calculated to be 17%,

suggesting amorphous properties. Also, the absence of off-axis peaks indicates structural disorder in the lattice. The DSC scan with a heating rate of 10 ℃/min shows its melting point at ~284 ℃ with the melting enthalpy of 17.4 J/g. Therefore, although PDPP3T shows semicrystalline melting characteristic, its molecular packing and ordering extend only over a short-range. Another example is P(NDI2OD-T2) (also known as N2200), which not only shows higher order (*h*00) peaks, but also exhibits (001), (002), (003) backbone peaks in GIWAXS 2D patterns, indicating good molecular packing. (NB: The absence of (00*l*) peaks in many other materials might not be due to disorder along the backbone, but a lack of scattering contrast between backbone moieties.) However, all peak widths reflect less than 10 layers of packing in each direction, including in the π-stacking direction. Accordingly, P(NDI2OD-T2) is classified as 2D semi-paracrystalline. We advocate that the most appropriate qualitative terminology to describe the spatial extent of the molecular packing is "2D paracrystallite". We note though that this classification is based on the assumption that lattice parameter fluctuations are not contributing significantly to the peak broadening that the *g* parameter calculated measures the paracrystalline, *i.e.*, cumulative, lattice disorder.

In summary, we classified the semiconducting polymers into five categories: 3D amorphous, oriented amorphous, highly disordered, 2D semi-paracrystalline, and 3D semi-paracrystalline. 3D amorphous polymers only show less than three molecular layers of stacking with $g \geq 12\%$ in all directions and exhibit only a T_g without T_m in DSC. Highly disordered polymers show similar characteristics with 3D amorphous ones except that the orientation distribution is not completely isotropic and some preferred edge-on or face-on population is present (the detailed analysis of this distributions warrants a separate review and is not included here). The semi-paracrystalline polymers show a melting transition in DSC and higher order diffraction peaks in GIWAXS with at least one direction of $g < 12\%$. For 2D semi-paracrystalline polymers, the *g* parameter for the least ordered direction is still $\geq 12\%$, resulting in 2D ordered platelets. In contrast, the *g* parameters are less than 12% in all three directions for 3D semi-paracrystalline polymers. Still, there are also some conundrums that need to be resolved in the semiconducting polymer fields.

4. Toward Polymer Crystals with *g* <5% and Long Coherence Length

The prior section has made it clear that even the most highly ordered semiconducting polymers to date have a *g* parameter of >6% in the π-π direction, and then the question is: Can semiconducting polymeric materials with significantly lower *g* parameters be designed? In this section, we are going to discuss the challenging tasks of pursuing large crystals and near-perfect semiconducting polymer crystals with low lattice disorder and possible approaches to achieving these goals.

4.1 Why it is Essential to Pursue Perfect Polymer Crystals

The molecular and mesoscale order of semiconducting polymers has been extensively studied and correlated with the charge transport properties, such as the exciton diffusion length and charge mobility, which are essential for high-performance devices. It is reported, for example, that the exciton diffusion length is a monotonic function of the extent of molecular order and its impact on energetic disorder[104]. X. Jin *et al.*[105] recently reported that the exciton diffusion length can be as high as 200 nm in conjugated polymer nanofibers prepared by seeded growth to form well-ordered domains with increased molecular ordering and low energetic disorder. On the other hand, the charge mobility and material conductivity, are also reported to be related to the molecular order, such as the π-π stacking distance[106], the coherence length[107, 108], and the DoC[106]. The charge mobility can vary by several orders of magnitude and the highest charge mobility can be found in single crystals[109]. Forming a perfect crystal is an essential way to improve the charge transport properties of these polymers.

However, the crystallites formed by polymeric materials deviate substantially from perfect crystals, lacking ordering in one or two crystallographic axes. Also, the coherence length of the π-π stacking is generally reported to be only tens of intermolecular spacings even in the best cases. The lack of ordering in the π-stacking direction is particularly detrimental, given that an increase in L_c and DoC along the lamellar stacking direction has little impact on the electron transport properties due to the insulating nature of the solubilizing side chains[110]. Interestingly, Carpenter *et al.*[26] reported recently that the lamellar packing of FTAZ with appropriate processing can exhibit a highly ordered side-chain layer and lamellar ordering with a coherence length >70 nm (limited by instrumental broadening) that corresponds to more than 150 intermolecular lamellar spacings. This opens up an opportunity and possibility to pursue crystals with long-range molecular order in all

directions, including backbone and π-stacking, if this ordering can be achieved synergistically for the backbone and sidechains.

4.2 Challenges of Achieving Perfect Crystals: 2D Crystalline Platelets and Nanocomposites

Although mesoscale ordering and texture in semiconducting films are also very important[111-113], these factors are complex and warrant their own review. Here, we will focus on molecular level interactions and ordering.

A perfect crystal of semiconducting conjugated polymers is expected to show excellent ordering along all three crystallographic axes, which are the π-π stacking direction, side-chain lamellar packing direction, and the backbone direction. In such cases, a unit cell is well defined. However, high level or paracrystalline disorder is prevalent even in the best cases. This must ultimately be connected to the chemically and structurally dissimilar nature and function of the backbone and side chains. In essence, these materials are "amphiphilic" by design, with the sidechains solely introduced to provide improved solubility. The ordering along the backbone and π-stacking directions in such "amphiphilic" materials are not necessarily achieved synergistically with ordering in the lamellar stacking direction or ordering between alkyl side chains. The competing interactions in the presence of structural, covalent constraints lead to frustration that is the most likely underlying factor that prevents crystal formation and leads to small coherence ellipsoids and the general inability to determine unit cells.

Early indications of the importance of solid (ordered) versus liquid (disordered) sidechains were observed in the paracrystalline to liquid crystalline transition of PBTTT, which was attributed to ordered *vs.* disordered sidechains and sidechain *vs.* backbone competition in a variety of semiconducting conjugated polymers. FTAZ, which we classified above in spun cast films as an highly disordered polymer with $g_{(010)}$=19% can, for example, under certain processing conditions (*e.g.*, drop-cast with high boiling point solvent) exhibit unusually long L_c for lamellar ordering that induces significant torsional backbone disorder, resulting in a multilayered nanostructure consisting of the ordered sidechain layers alternating with disordered backbone layers[26]. The sidechain ordering in FTAZ had characteristic GIWAXS, DSC, optical and near edge x-ray absorption fine structure (NEXAFS) signature. Upon melting of the highly ordered sidechain

nanophase, the backbones are no longer torsionally constrained and thus able to π-stack more efficiently. This form of a nanolayered structure, with some order in the backbone layer but disorder in the side-chain layer, is what is typically produced in spin-cast FTAZ films. NEXAFS spectroscopy could directly demonstrate this competing ordering, as shown in **Figure 8**. The NEXAFS spectra of drop-cast FTAZ (**Figure 8a**) show two characteristic peaks at 287.4 and 288.1 eV, corresponding to C 1s → σ^*_{C-H} transitions of trans conformations that agree well with the published NEXAFS for a nonadecane crystal[114]. This demonstration of the high degree of sidechain ordering is further corroborated by strong angular dependence of the NEXAFS intensity. Considering the C 1s → $\pi^*_{C=C}$ NEXAFS transition region of ~283.5-287 eV related to the backbone, only a single, broad peak is observed with limited angular dependence. This suggests a disordered backbone with near random orientation distribution. In contrast, the NEXAFS spectra of spin-cast FTAZ (**Figure 8b**) show the opposite characteristics with highly ordered backbone (splitting peak in the C 1s → $\pi^*_{C=C}$ transition that exhibit angular dependence) but disordered sidechain with a single peak for the C 1s → σ^*_{C-H} transitions that do not exhibit any angular dependence. Similar NEXAFS characteristics are observed in PCDTBT (**Figure 8e**), P(NDI2OD-T2) (**Figure 8g**) and P3HT films. Additionally, the GIWAXS pattern of drop-cast FTAZ exhibits a strong, sharp feature at ~1.47 $Å^{-1}$, highlighted with red arrow in **Figure 8c**, indicating the high degree of sidechain ordering, while these features are not present in spun-cast FTAZ film (**Figure 8d)**. These characteristic features for high degree of sidechain ordering are also present in drop-cast PCDTBT (**Figure 8f)** and P(NDI2OD-T2) (**Figure 8h)** films, but not in spin-cast films (not shown here). The competition between the sidechain and the backbone ordering with characteristic NEXAFS and GIWAXS characteristics is also observed in PCDTBT, P(NDI2OD-T2) and P3HT films and might, therefore, be a general feature of most semiconducting materials to date. This indicates that expectations of molecular packing with a well-defined unit cell are maybe misplaced and that most current materials have to be considered nanomaterials with alternating ordered and disordered layers. The general lack of observing the characteristic features for alkane ordering in most GIWAXS data indicates that most processing conditions lead to a disordered alkane nanolayer.

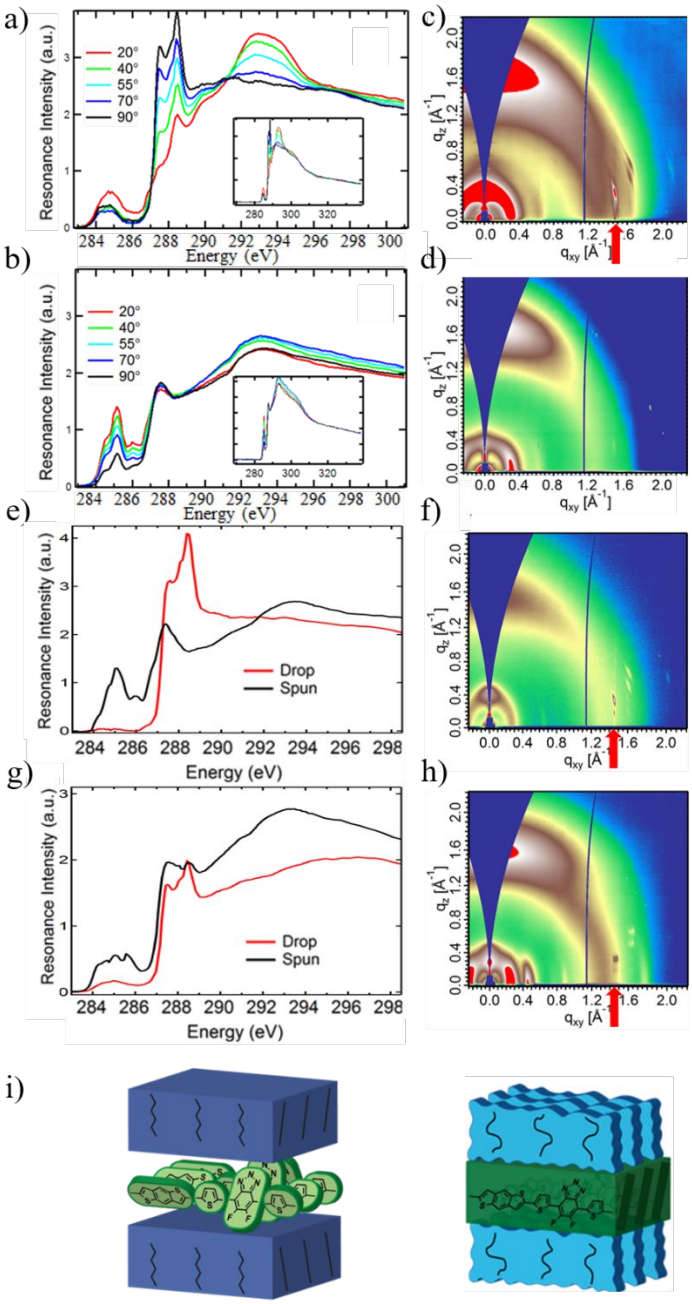

Figure 8. NEXAFS spectra that demonstrate the competition between backbone ordering and sidechain ordering and GIWAXS patterns that show the high degree of sidechain ordering for drop-cast thin films from chlorobenzene[26]. Reproduced with permission from ref. 26. The NEXAFS spectra for a) drop-cast FTAZ and b) spin-cast FTAZ, where 90° is normal incidence. GIWAXS patterns for c) drop-cast FTAZ and d) spin-cast FTAZ. NEXAFS spectra at normal incidence of drop-cast and spin-cast films of e) PCDTBT, and g) P(NDI2OD-T2). 2D GIWAXS patterns from drop-cast films of f) PCDTBT, and h) P(NDI2OD-T2). The sharp features at ~1.47 Å^{-1} highlighted with red arrows in drop-cast films indicate the

high degree of sidechain ordering. i) The demonstration of the competition between the backbone ordering and the side-chain ordering.

4.3 Possible Approaches Towards Single Crystals with Low *g* Parameters

Although a lot of challenges still existing in pursuing the creation of perfect crystals, there are some possible solutions. Two aspects need to be separately considered: 1) the mesoscale size of ordered domains and DoC one can achieve, and 2) molecular packing and its lattice disorder as captured in the *g* parameter. The mesoscale order is often impacted by kinetic and external factors. However, it should generally be coupled to the molecular packing. The lower the *g* parameter, the larger the paracrystallites and the easier it should be to achieve macroscopically ordered domain and high DoC.

Solvent engineering is a facile approach to induce mesoscale ordering for paracrystalline polymers, in which ordered domains, similar to the PE crystals discussed above, are composed of micro-paracrystals aligned together. For instance, Müller *et al.*[115] induced macroscopic-sized, highly ordered domains of P3HT (**Figure 9a**) via a mixture of crystallizable solvent 1,3,5-trichlorobenzene (TCB) and a second carrier solvent such as chlorobenzene. The solidification was initiated by growth of macroscopic TCB spherulites and followed by replicated epitaxial ordering of a variety of conjugated polymers, such as P3HT and PCPDTBT, on TCB crystals. When TCB is removed, the macroscopic-sized P3HT or PCPDTBT spherulites were left behind. Except for the enlarged size of the ordered domains, the induced spherulites also show more preferentially face-on orientation and the paracrystallites have a smaller *g* parameter for the π-π stacking as inferred here from the narrower diffraction peaks as published. Another way to improve the mesoscale order is strain-induced alignment. Jimison *et al.*[116] reported that P3HT can be directionally crystallized over micrometers (**Figure 9b**) with the help of TCB, which at first acts as a solvent and then as a substrate for polymer epitaxy after TCB solidifies in characteristic needle-like crystals.

The coupling of mesoscale and molecular ordering was also observed by X. Jin *et al.*[105] that a well-ordered semiconducting nanofiber core with a solvated, segmented corona with polythiophene at the nanofiber ends (**Figure 9c**), exhibit unusually high exciton diffusion and charge transport

properties. The improvement is correlated with the increased molecular ordering for the conjugated polymer as observed by WAXS and the pronounced vibronic structure and narrow spectral linewidths in the photoluminescence. The relationship of molecular ordering to molecule design was nicely elucidated by B. Kang *et al*.[117], demonstrating that the molecular packing of PNDIF-T2 and PNDIF-TVT are dominated by the strong self-organization of the semifluorinated sidechains with a tight interdigitation of antiparallel sidechains rather than by the interactions between the backbones. In PNDIF-T2, the strong self-organization of the sidechains lengthens the polymer backbone from 14.3 Å (DFT expectations) to 15.8 Å (experiments). The *d*-spacings along the backbone direction are further extended to 16.2 Å with the use of 1-chloronaphthalene additive. This extension of the polymer chains along the backbone changes the dihedral angles between the repeating units driven by the closely packed hexagonal structure of the fluorinated sidechains as shown in **Figure 9d**.

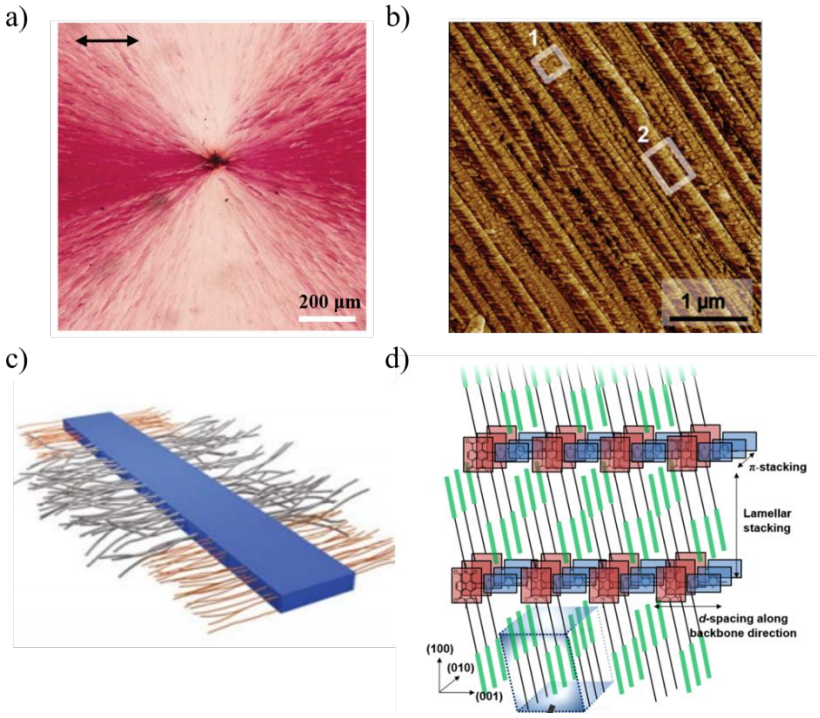

Figure 9. a) The spherulite-like structure of P3HT formed as a replica of the original TCB spherulites[115]. Reproduced with permission from ref. 115. b) The micrometer-sized directionally crystallized P3HT induced by mechanical strain[116]. Reproduced with permission from ref. 116. c) Schematic of the highly ordered nanofibers formed with the seeded growth process[105]. Reproduced with permission from ref. 105.

d) The closely packed structure of PNDIF-T2 via side-chain-induced self-organization[117]. Reproduced with permission from ref. 117.

4.4. Required Synthetic Controls

Highly ordered crystallites require highly controlled synthesis. The importance of stereochemistry has been long recognized and is exquisitely exemplified by the differences between regiorandom and regioregular P3HT, where the former is 3D amorphous while the latter one is of the most highly ordered materials. Sidechain interdigitation provides a mechanism for three-dimensional ordering. However, high sidechain attachment density prevents sidechain interdigitation and long-range intermolecular organization. For example, the sidechain density in P3HT is too large to permit interdigitation when the backbone is well packed[118] and mostly results in two-dimensionally ordered, smectic-like structure without registry between layers. In contrast, the side-chain attachment densities of PBTTT and PQT are sufficiently low to permit the interdigitation of side chains, which preserves the packing structure by interlocking adjacent layers and thus promote three-dimensional order[119].

For push-pull copolymers, packing defects can occur when head-to-head synthesis disrupts the creation of a perfect alternating copolymer. Such defects have been beautifully visualized in the case of C_{14}DPPF-F[120]. The high-resolution scanning tunneling microscopy (STM) image of C_{14}DPPF-F polymer on Au(111) indicates straight and tightly aligned polymer backbones and the interdigitation of the alkyl side chains. However, there are also darker gaps in the interdigitation sequence of side chains, highlighted with the white arrows in **Figure 10a**. Since the STM image displays a periodic sub-molecular contrast, the features in the STM image can be identified with the corresponding chemical structure of C_{14}DPPF-F as described in **Figure 10c.** At the position of the gaps, the model is inverted through a mirror plane perpendicular to the polymer backbone (**Figure 10b**), resulting in an ABBA monomer sequence instead of the regular ABAB sequence, where A monomer refers to DPPF unit and B monomer is the furan (as shown in **Figure 10d**). The schematic demonstration in **Figure 10e-h** also shows that the resulting gaps in the sidechain interdigitation with ABBA sequence (**Figure 10h**) will result in similar gaps with actual defects shown in the STM image. These chemical defects result from the homocoupling between the DPP-containing units, which implies that new synthetic strategies are required to avoid these defects.

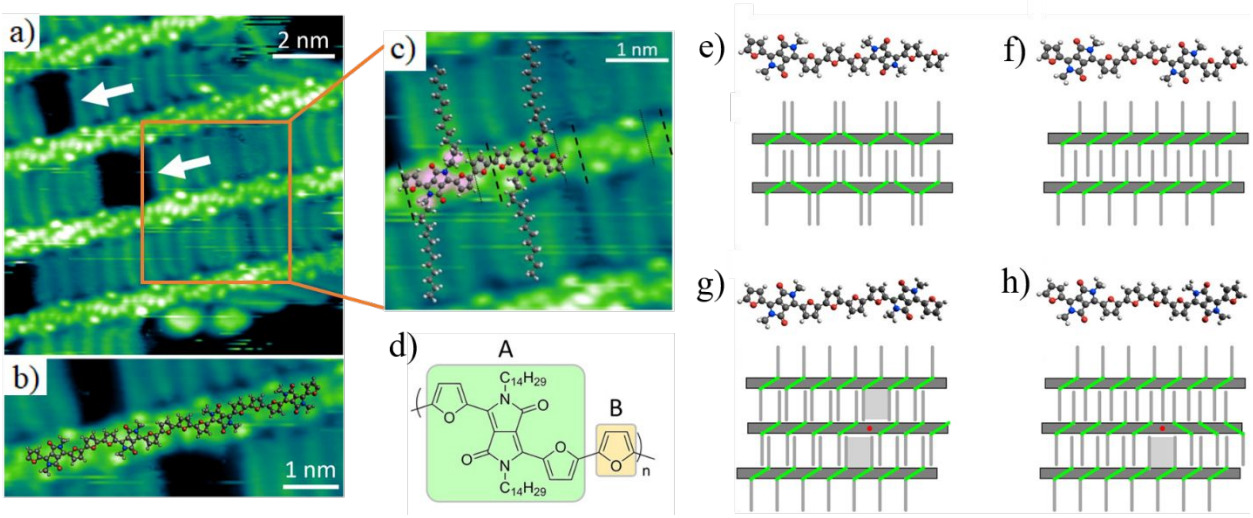

Figure 10. a) High-resolution scanning tunneling microscopy (STM) image of C_{14}DPPF-F polymer on Au(111) of polymer backbones and interdigitation of the alkyl side chains. White arrows indicate gaps in the sidechain interdigitation. The molecular model is superposed onto part of the central polymer strand indicating the backbone in b) and the side chain interdigitation in c) (where C atoms are shown in gray, O in red, N in blue, and H in white). d) Molecular structure of C_{14}DPPF-F with the identification of the individual monomer units: DPPF (A) and furan (B). Structure and schematic representation (with alkyl chains by thin gray lines, and the DPP units by green segments) of defect-free C_{14}DPPF-F in the all-trans configuration in e) and with a single furan-furan cis arrangement in f). Structure and schematic representation of C_{14}DPPF-F around an ABBA defect in the all-trans configuration in g) and with a single furan-furan cis arrangement in h). The ABBA defects are represented by red dots, and larger gaps in the chain interdigitation are represented by gray-shaded areas. Adapted with permission from ref. 120. We note that the molecules might be distorted relative to a bulk environment due to confinement to the surface.

Given the interplay of sidechain ordering and backbone ordering, defects or uncontrolled chemical structure in the sidechains might also be problematic and prevent perfect crystal formation. To some extent, it might not be surprising that the lowest *g* parameters have been achieved with unbranched sidechains and that the use of branched sidechains to improve solubility might be detrimental to structural order. Carpenter *et al.*[26] thus speculated that stereochemistry control even in the branched sidechains might be the key for perfect ordering for high performance and to explore a synergistic ordering of the backbone and sidechain. This stereochemistry control is also favored by D. Venkateshvaran *et al.*[121] that the charge transport in IDTBT approaches intrinsic

disorder-free limits with all molecular sites thermally accessible due to the molecular packing with planar, largely torsion-free backbone and disordered, non-interdigitated sidechain arrangement.

5. Conceptual Graft Hetero-epitaxy of Backbone onto Sidechain Crystals: A New Molecular Design Perspective

In this final section, we attempt to provide some perspective and propose a forward-looking conceptual idea; a new molecular design paradigm to make perfect polymer crystal possible by conceptual backbone "graft hetero-epitaxy" onto side-chain crystals. We note that only a few semiconducting polymers have been synthesized that are 3D semi-paracrystalline, all of which still have *g* parameters > 6% in at least one direction. We deduce from the preponderance of the literature and the discussion above that poor ordering is due to the intrinsic molecular design, and specifically due to the current incommensurability of the ideal sidechain spacing defined by the crystalline state of the sidechains with the spacing determined by the available or convenient synthesis attachment points along the backbone. In other words, the spacing and density of the attachment points of the sidechains for a layer of perfectly ordered backbones do rarely correspond to the spacing and density in a fully ordered, crystalline sidechain layer.

Examples about the two most ordered semiconducting polymers, P3HT and PBTTT, are provided to demonstrate the incommensurability of the sidechain spacing with the attachment points in the polymer backbone. The primitive unit cell of P3HT packing is commonly described as orthorhombic[103, 122] although the monoclinic structure is also proposed[82, 102, 123]. Colle *et al.*[122] investigated the regio-regular head-to-tail P3HT (rr-HT-P3HT) by minimizing the total electronic energy with respect to all the geometrical parameters of the system with DFT and show that the minimum energy structure of the crystalline P3HT corresponds to a lattice of almost orthorhombic primitive cells with a = 16.7 Å, b = 7.5 Å, c = 7.9 Å, with the molecular packing shown in **Figure 11a**, which contain two non-equivalent polymer chains. The proposed monoclinic unit cells are obtained by selected area electron diffraction (SAED) for regioregular P3HT by directional epitaxial solidification in TCB with a = 16.0 Å, b = 7.8 Å, c = 7.8 Å, γ = 93.5°[102] or = 86.5°[82]. However, if the side chain of P3HT could freely crystallize into an alkane crystal of C_6H_{14}, they would exhibit a triclinic structure[124] with unit-cell parameters of a = 4.17 Å, b = 4.70 Å, c = 8.57 Å, α = 96.6°, β = 87.2°, γ = 105.0° (The n-hexane crystals were grown in sealed capillaries of

Lindeman glass with desired low temperature by liquid nitrogen). Therefore, the unit cell of the alkane crystals does not match with that of the unit cell of the polymer backbone. Similar situation of the mismatch is also present in PBTTT. The unit cell of PBTTT is reported to be triclinic, as shown in **Figure 11c**, with a = 19.6 Å, b = 5.4 Å, c = 13.6 Å, α = 136.0°, β = 84.0°, γ = 86.0° for PBTTT-C_{12}[58] and a = 21.5 Å, b = 5.4 Å, c = 13.5 Å, α = 137°, β = 86°, γ = 89° for PBTTT-C_{14}[125]. On the other hand, the unit cell of the alkane crystals are both triclinic with a = 4.28 Å, b = 4.81 Å, c = 17.32 Å, α = 83.27°, β = 66.13°, γ = 74.00° for $C_{12}H_{26}$, a = 4.29 Å, b = 4.82 Å, c = 19.84 Å, α = 84.10°, β = 66.82°, γ = 73.00° for $C_{14}H_{30}$, which are predicted based on the unit-cell parameters of n-octadecane crystals[126]. Importantly, the results of Carpenter *et al.*[26] have shown that the sidechain ordering can dominate energetically over the backbone ordering at room temperature in cases such as FTAZ where the distortions of the backbone must be energetically rather costly.

We suggest that this strong ordering of the sidechains should be exploited and that the design and synthesis of semiconducting polymers borrow the concepts of heteroepitaxy from compound semiconductor thin film growth. It is likely instructive and advantageous to reverse the design considerations. While it is the backbone design that is currently contemplated first prior to synthesis and then various sidechains are attached in purely trial-and-error fashion wherever synthetically convenient, the reverse design process that starts with the sidechains might be interesting if not tantalizing to consider.

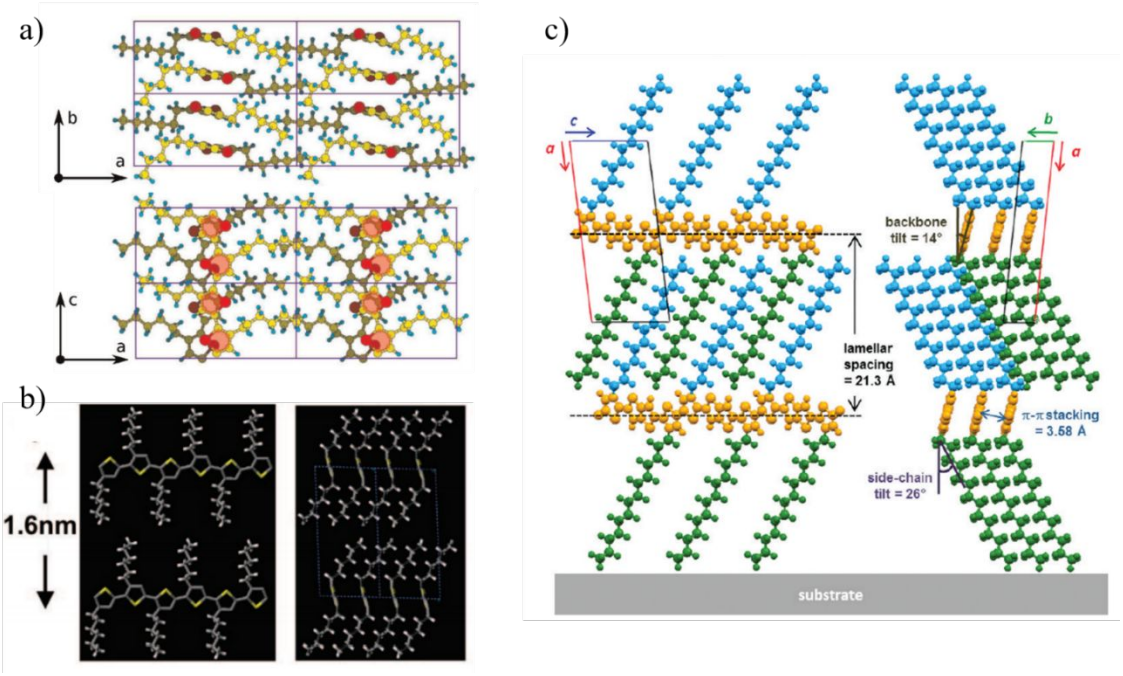

Figure 11. a) The packing of orthorhombic unit cell of the crystalline rr-HT-P3HT polymer. Reproduced with permission of ref. 122. b) The packing of monoclinic unit cell of rr-P3HT seen along the *b* and *c* axis. Reproduced with permission of ref. 123. c) The schematic illustration of the triclinic unit cell of PBTTT-C_{14}. Reproduced with permission of ref. 126.

Let us create a conceptual perfect 2D crystal layer of sidechains *in-silico* of which the unit cell parameters as well as the space-group can be varied by the length and nature of the sidechains (alkene, ethylene glycol, floriated alkanes, *etc.*), as illustrated in **Figure 12c**. Subsequently, we design a backbone and possible linkers *in-silico* to conceptually graft the backbone commensurably with this perfect alkane layer in such a way that the backbone is also perfectly ordered. In **Figure 12a**, it is illustrated that if the size and density of attachment of backbone moiety are not commensurate with the lattice parameter of sidechain crystals, the backbone will be compressed or stretched, and thus the backbone ordering is reduced. If there is commensurability between the backbone and sidechain packing, as illustrated in **Figure 12b**, the backbone and sidechain ordering can be reached synergistically. A material designed in this way should readily order into 3D crystals. Most excitingly, the side-chain crystals might be used to straighten or even strain the backbone or to control the π-π stacking with a controlled sliding distance. This paradigm, if geometrically allowed by nature, might allow totally new ways of designing electronic properties in the 2D (001)-(010) layers created by the backbone that are

separated by an insulating layer of sidechains. We note here that use of any branched sidechains without control of stereochemistry would likely destroy the ability to achieve “hetero-epitaxy”.

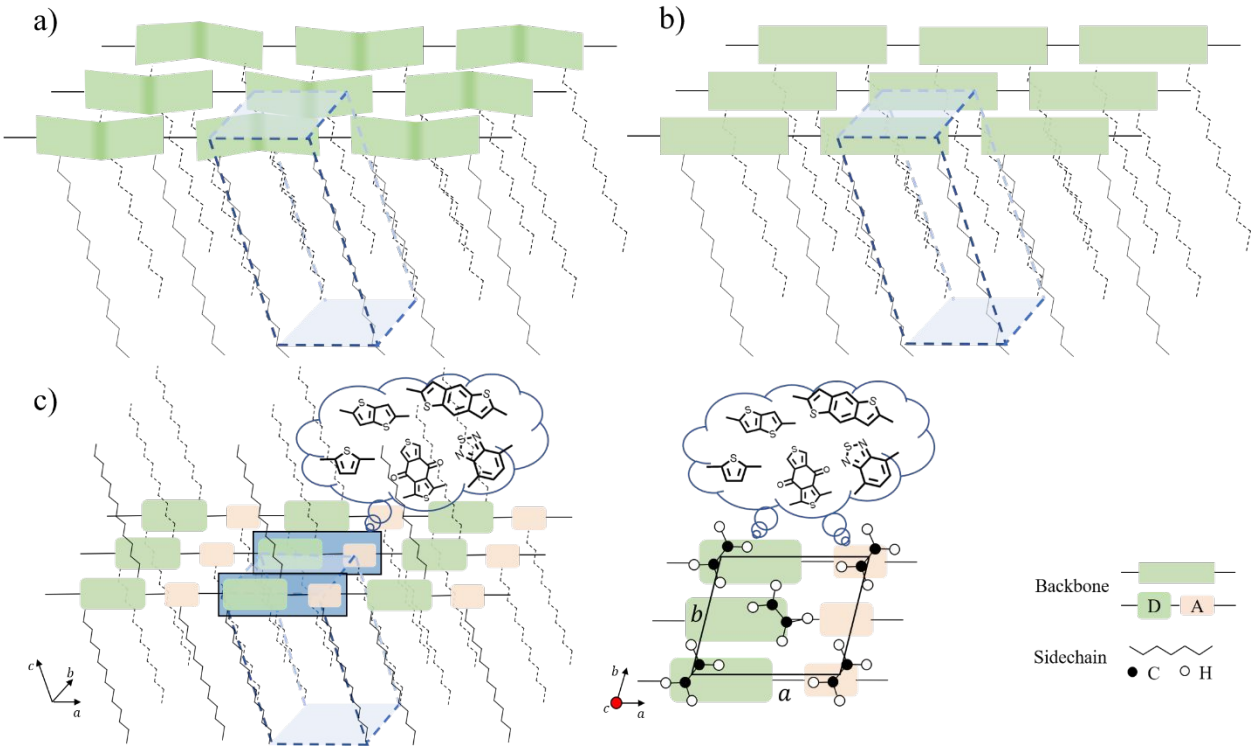

Figure 12. Schematic illustration of the graft hetero-epitaxy concept for the chemical structure design for conjugated polymers. With the unit-cell parameter of a perfect alkane crystal of sidechains, the sidechain attachment points at the backbone are determined. a) When the size and density of attachment of backbone moiety are not commensurate with the lattice parameter of sidechain crystals, the backbone is compressed or stretched, and thus the backbone ordering is reduced. b) If there is commensurability between the backbone and sidechain packing, the backbone and sidechain ordering can be reached synergistically, making it possible to reach perfect conjugate polymer crystals. To demonstrate how to design this commensurability, c) shows the design strategy that the backbone moieties need to be carefully chosen or designed to match with the size and density of attachment points, dihedral angle, etc. of the alkane crystal of sidechains.

Summary and Outlook

In this review, we have clarified qualitative nomenclature related to molecular order that are commonly used in the organic electronics, such as crystalline, semicrystalline, paracrystalline,

amorphous, crystallinity, crystallites, and paracrystallites, and advocated at times for a specific usage. With the help of GIWAXS and DSC, one can in most cases identify the molecular packing of semiconducting polymers ranging from 3D amorphous to 3D semi-paracrystalline. We specifically advocate that GIWAXS peak shape analysis is performed and that values for *g* parameters are broadly reported to allow for a more consistent use of terminology and comparison between materials and the literature at large. We have also contemplated how to improve the molecular ordering of the semiconducting conjugated polymers to approach perfect crystals as an essential way to improve the charge transport properties and thus the device performance. Although there are lots of unsolved problems, further advances in semiconducting conjugated polymer design and synthesis might lie in the proposed hetero-epitaxy concept and stereochemistry control to explore the synergistic ordering of both the backbone and the sidechains in thermodynamically favorable packing configurations or tune the side chain crystallinity and interdigitation to provide a mechanism for three-dimensional order, improving the ordering and thus yielding higher performance.

In summary, we would like to provide a few highlights about semiconducting polymers.

- Semiconducting polymers are 3D semi-paracrystalline at best for the reported materials to date.

- When finite size dominates the diffraction peak broadening, the Scherrer equation is a good estimation of crystallite size. When paracrystalline disorder dominates the diffraction peak broadening, the coherence length from Scherrer equation reflects the length scale of paracrystalline ordering. If lattice parameter fluctuation dominates the diffraction peak broadening, we cannot make any conclusion on the crystallite size or the size of paracrystalline disorder from single peak analysis.

- Coherence ellipsoid is suggested as a useful concept to take account of the different coherence lengths in different packing directions, particularly the (100) and (010) directions. This concept has been used to create the new class of 2D paracrystals, which can be visualized as ordered platelets.

Glossary

Amorphous: Amorphous materials are characterized by the absence of molecular ordering and any melting peak in DSC. Here, we classify the amorphous materials into three types, 3D amorphous, oriented amorphous and highly disordered, all of which do not show melting peak in DSC scans. For 3D amorphous materials, it is scattered diffusely in X-ray diffraction experiments with broad and isotropic scattering peaks corresponding to only 2-5 molecular layers and a *g* parameter ≥12%. For oriented amorphous/highly disordered materials, the scattering peaks are also broad while there is some preferred orientation of segments in a certain direction. T_g is observable for 3D amorphous and oriented amorphous films with conventional DSC while not for highly disordered films.

Backbone ordering: the ordering along the chain backbone direction. If there is strong chain extension of conjugated polymers, the backbones show an ordered alignment, resulting in corresponding diffraction peaks.

Bragg reflection: the reflection that satisfies Bragg condition, $2d\sin(\theta/2) = n\lambda$, where d is the stacking distance, θ is the diffraction angle, λ is the wavelength of the X-ray and n is an integer called the order of diffraction.

***Coherence length* (L_c)**: It is a measure of the size of ordered regions (*e.g.*, crystallites) that can be diffracted coherently. It is related to peak width via Scherrer equation: $L_c=2\pi K/\Delta q$, where K is a shape factor (typically 0.8-1) and Δq is the FWHM of a diffraction peak.

Conformational freedom: The spatial or structural arrangement of atoms affording distinction between stereoisomers can be interconverted by rotations about formally single bonds, *e.g.*, the planar *vs.* twisted backbone chains.

Configurational freedom: The spatial relation of atoms in the molecule is not fixed, *e.g.*, different chirality or tacticity, *cis*- *vs. trans*- configuration.

Column Length: refers to crystallite size emphasizing on the length of a column of unit cells stacked along the normal of the diffracting lattice planes (diffraction vector).

Crystalline: Crystalline state is characterized by three-dimensional, long-range positional order on an atomic scale.

Crystallite: the ordered domains with small size on the order of 1-100 nm.

Crystallinity: degree of crystallinity (DoC), the volume fraction of crystalline domains in semicrystalline films.

***Cumulative disorder*:** the distortions and defects that can be accumulated, resulting in the loss of predictive ability regarding the position of a unit cell as the displacement along a certain direction of a lattice increases. The most contributing term is paracrystalline disorder**.**

Debye-Waller factor: a kind of noncumulative lattice disorder, directly related to static or dynamic components of atomic mean-square displacement, defined as $e^{-(kq)^2/4\pi^2}$ where q is the scattering vector, k is the average root-mean-square displacement of atoms from their position in a crystalline lattice. It can be used to describe the attenuation of x-ray scattering or coherent neutron scattering intensity caused by thermal fluctuation and lattice imperfection.

Defect: The defect in a crystal includes point defects, linear defects, and planar defects. Point defects refer to places where an atom is missing or irregularly placed in the lattice structure, including vacancies and impurity. Linear defects (or dislocation) are groups of atoms in irregular positions. Planar defects are interfaces between homogeneous regions of the material, such as grain boundary.

d-spacing: the interplanar spacing, d_{hkl}, defined as the spacing between successive (*hkl*) planes. It can be calculated by the reciprocal of the peak position (q) with $d = 2\pi/q$. A knowledge of peak indices and their corresponding *d*-spacings can be used to refine unit cell parameters.

DSC: differential scanning calorimetry, a thermal analysis technique characterizing how a material's heat capacity is changed with temperatures. It can be applied to detect thermal transitions such as the glass transition (T_g), crystallization (T_c) and melting (T_m) associated with disordered and ordered phases of the sample.

Enthalpy of fusion: the change in the enthalpy resulting from providing energy, typically heat, to a specific quantity of the substance to change its state from a solid to a liquid, at constant pressure.

Ewald sphere: Ewald's sphere is constructed with the radius defined by the incoming $\overrightarrow{k_o}$ vector and centered at the origin of $\overrightarrow{k_o}$ (the illustration please see **Figure 3b**). The diffraction condition can be met when Ewald sphere intersects with a given crystallite orientation sphere. Ewald sphere is useful for comparing different diffraction geometries.

Fiber texture: There is only out-of-plane orientation preference with no in-plane orientation preference.

FWHM: full width at half maximum of a given diffraction peak. It is one kind of description of peak width.

Gaussian distribution: normal distribution, a type of continuous probability distribution for a real-valued random variable. The general form of its probability function is $f(x) = \frac{1}{\sigma\sqrt{2\pi}} e^{-\frac{1}{2}(\frac{x-\mu}{\sigma})^2}$, where μ is the mean of the distribution and σ is its standard deviation.

GIWAXS: grazing-incidence wide-angle X-ray scattering, a structural measurement technique wherein wide-angle scattering and molecular length scales are collected.

g parameter: paracrystalline disorder parameter, a measure of the percentage of statistical deviation from the mean lattice spacing in a crystal. It is defined with interplanar spacing *d* as: $g^2 = (< d^2 > - < d >^2) / < d >^2$.

Hetero-epitaxy grafting: the growth of a crystalline film based on a well-defined orientation with respect to the crystalline substrate of a different material. Here, we borrow this concept to refer to a proposed conjugated polymer design strategy that the backbone moieties are chosen or designed to be commensurate with the lattice parameters of sidechain crystals.

Integral breath: defined as the integral intensity of a peak divided by the maximum intensity /peak height. It is one kind of description of peak width.

Lattice parameter fluctuations (e_{rms}): the variance of the interplanar spacing within a sample from one crystallite to the next, from one area of the diffracting volume to another. It characterizes inhomogeneities within a sample, such as a slight contraction or expansion of the lattice spacing due to appearance of interfaces.

Line shape analysis: an analysis based on trends of peak widths and Lorentzian components of pseudo-Voigt line shapes as a function of diffraction orders. The peak width as a function of peak order can help distinguish the contribution of finite size from the lattice disorder to the broadening of peaks while the Lorentzian components of pseudo-Voigt line shapes is a good way to determine the paracrystalline disorder from lattice parameter fluctuation.

Liquid crystalline: Liquid crystalline phase is a mesophase with positional dynamic disorder but some long-range orientational order. The exothermic or endothermic enthalpy for crystallization or melting in liquid crystalline films is independent of the cooling/heating rate. Liquid crystalline films show a birefringent phase when viewed between crossed polarizers in a polarization microscope. The alignment of polymer chains can be enhanced by thermally annealing as-cast films into liquid crystalline mesophase to form closely packed structure.

Lorentzian distribution: also known as Cauchy distribution. It is a continuous distribution with probability distribution function given by: $f(x;x_0,\gamma) = \frac{1}{\pi}(\frac{\gamma}{(x-x_0)^2+\gamma^2})$, where x_0 is the location of the peak of the distribution and γ is the scale parameter specifying the half the width at half the maximum height.

Morphology: characterizing the nanostructure or microstructure of a bi-continuous network of domains in terms of molecular packing and phase separation.

NMR: nuclear magnetic resonance. When nuclei in a strong constant magnetic field are perturbed by a weak oscillating magnetic field, an energy transfer is possible between the base energy to an excited energy level and then emit an electromagnetic signal with the same frequency when it returns to the base energy level. NMR is sensitive to local chemical environment and thus used to probe local interaction and ordering.

Noncumulative disorder: random statistical fluctuations about an ideal lattice position.

Number of stacking layers (n): characterized by the ratio of the coherence length and the stacking distance of a certain diffraction peak.

Paracrystalline: Paracrystalline state is an intermediate state between crystalline and amorphous. In paracrystalline phase, the distances between atoms in the space lattice are not constant but show correlated statistical fluctuations in both the direction of neighboring atoms and perpendicular to it, preventing long-range order. Paracrystals follow the empirical α□-law, which restricts their size. The paracrystalline disorder is quantified by paracrystalline disorder parameter *g*.

Pole figure: A pole figure is a graphical representation of the variation in diffraction intensity with respect to directions in the specimen, providing information on the texture. For a fiber texture, pole figures describe the orientational distribution of the diffracted intensity of a chosen diffraction peak as a function of all possible crystallite orientations with polar angles χ from -90° to 90° where χ is defined as the angle between the scattering vector and the substrate normal and χ=0° refers to the out-of-plane direction. Pole figure can be used to calculate DoC and face-on/edge-on ratio.

Pseudo-Voigt mixing parameter η: the fraction of Lorentzian function in a Voigt profile. η = 0 represents a Gaussian line shape while η = 1 represents a Lorentzian distribution.

P-SoXS: soft x-ray scattering with polarized light. P-SoXS is sensitive to bond orientation which lies on the orientational material contrast between the cases where the average dipole moment is aligned parallel or perpendicular to the incident electric field.

Resolution: Smearing of the diffraction peaks by beam size, divergence, and beam footprint on the sample. The latter term gives rise to geometric smearing which becomes broader with scattering angle and is a specific challenge in GIWAXS. The overall resolution is often well described as a Gaussian function and has to be taken into account for Scherrer analysis and peak shape analysis.

Semicrystalline: partially crystalline. Semicrystalline materials are composed of ordered domains but also a volume fraction of amorphous domains.

Semi-paracrystalline: partially paracrystalline. Semi-paracrystalline materials are composed of paracrystalline domains but also a volume fraction of amorphous domains.

Sidechain ordering: Side chains (for instance, alkyls) of conjugated polymers are ordered independently of the aromatic backbones to form separate nanophases.

Specific volume: the number of cubic meters occupied by one kilogram of matter, characterized by the ratio of the volume of a material to its mass.

Stacking distance (d): the distance between stacked planes. The commonly used ones in GIWAXS are the lamellar stacking distance and π-π stacking distance. With the assumption of simple orthorhombic unit cell, the lamellar stacking distance and π-π stacking distance are equal to d_{100} and d_{010}, respectively.

TEM: transmission electron microscopy, a microscopy technique where a beam of electrons is transmitted through a specimen to form an image. The interactions between the electrons and the atoms can be used to observe nanoscale features such as the crystal structure and features in the structure like dislocations and grain boundaries.

Texture: The crystallite alignment or orientation distribution with respect to the substrate normal, such as face-on *vs.* edge-on texture or fiber texture which is isotropic in-plane orientation.

Warren-Averbach framework: It employs the deconvolution Fourier-transform method for the determination of the intrinsic physical line profile. The shape of the diffraction peaks is represented by a Fourier series while calculated Fourier coefficients will be the product of two terms: the size contribution (independent of peak order) and the disorder coefficient (peak-order dependent). By decoupling these two terms, it can determine the contributions of finite size or lattice disorder to the peak broadening.

Williamson-Hall analysis: It assumes a pure paracrystal model where the ordered phases are paracrystalline, and thus only the paracrystalline disorder and the finite paracrystallite size

contribute to the peak broadening, ignoring the possible contribution from lattice parameter fluctuations. According to equation (7), with the plot of β *vs*. m^2, *g* parameter can be obtained from the slope and finite paracrystallite size from the intercept.

Appendix A: the full name of polymers involved in the review

C_{14}DPPF-F: Poly(tetradecyl-diketopyrrolopyrrole-furan-co-furan)

F8BT: Poly(9,9-dioctylfluorene-co-benzothiadiazole)

F8T2: Poly(9,9-dioctylfuorene-co-dithiophene)

FTAZ: Poly[(3-butylnonyl)benzodithiophene-co-fluorinatedtriazole]

P3HT: Poly(3-hexylthiophene-2,5-diyl)

P3EHT: Poly(3-(2'-ethyl) hexylthiophene)

P3DDT: Poly(3-dodecylthiophene)

PBDB-T: Poly[(2,6-(4,8-bis(5-(2-ethylhexyl)thiophen-2-yl)-benzo[1,2-b:4,5-b']dithiophene))-alt-(5,5-(1',3'-di-2-thienyl-5',7'-bis(2-ethylhexyl)benzo[1',2'-c:4',5'-c']dithiophene-4,8-dione)]

PBDT-TDZ: Poly[1,3,4-thiadiazole-(benzo[1,2-b:4,5-b′]dithiophene)]

PBDTS-TDZ: Poly[1,3,4-thiadiazole-2,5-diyl(3-octyl-2,5-thiophenediyl)[4,8-bis[(2-butyloctyl)thio]benzo[1,2-b:4, 5-b′]dithiophene-2,6-diyl](4-octyl-2,5-thiophenediyl)]

PBTTT: Poly[2,5-bis(3-tetradecylthiophen-2-yl)thieno[3,2-b]thiophene]

PDPP3T: Poly{2,2′-[(2,5-bis(2-hexyldecyl)-3,6-dioxo-2,3,5,6- tetrahydropyrrolo[3,4-c]pyrrole-1,4-diyl)dithiophene]- 5,5′-diyl-alt-thiophen-2,5-diyl}

PCDTBT: Poly[N-9'-heptadecanyl-2,7-carbazole-alt-5,5-(4',7'-di-2-thienyl-2',1',3'-benzothiadiazole)]

PffBT4T-2OD: Poly[(5,6-difluoro-2,1,3-benzothiadiazol-4,7-diyl)-alt-(3,3'''-di(2-octyldodecyl)-2,2',5',2'',5'',2'''-quaterthiophen-5,5'''-diyl)]

PM6: Poly[(2,6-(4,8-bis(5-(2-ethylhexyl-3-fluoro)thiophen-2-yl)-benzo][1,2-b:4,5 -b'] dithiophene))-alt-(5,5-(1',3'-di-2-thienyl-5',7'-bis(2-ethylhexyl)benzo[1',2'-c:4',5' -c']dithiophene-4,8-dione)

PMMA: Poly(methyl methacrylate)

P(NDI2OD-T2): Poly{[N,N'-bis(2-octyldodecyl)naphthalene-1,4,5,8-bis(dicarboximide)-2,6-diyl]-alt-5,5'-(2,2'-bithiophene)}

PQT: Poly(3,3'''-dialkylquaterthiophene)

PS: Polystyrene

PTAA: Poly(triaryl amine)

PTB7: Polythieno[3,4-b]-thiophene-co-benzodithiophene

PTB7-Th: Poly[4,8-bis(5-(2-ethylhexyl)thiophen-2-yl)benzo[1,2-b;4,5-b']dithiophene-2,6-diyl-alt-(4-(2-ethylhexyl)-3-fluorothieno[3,4-b]thiophene-)-2-carboxylate-2-6-diyl)]

PTQ10: Poly[[6,7-difluoro[(2-hexyldecyl)oxy]-5,8-quinoxalinediyl]-2,5-thiophenediyl]

TIPS-Pentacene: 6,13-Bis(triisopropylsilylethynyl)pentacene

Acknowledgements

The authors would like to acknowledge the support from the ONR grant N000141712204 and N000142012155. GIWAXS data were acquired at beamline 7.3.3 at the Advanced Light Source, which are supported by the Director of the Office of Science, Office of Basic Energy Sciences, of the U.S. Department of Energy under Contract No. DE-AC02-05CH11231. L.Y. also appreciates the National Natural Science Foundation of China (52073207) for support. The authors gratefully acknowledge Subhrangsu Mukherjee, Masoud Ghasemi, Indunil Angunawela for the acquisition of part of GIWAXS and DSC data and appreciate the fruitful discussions with Dean M. DeLongchamp (NIST), Obaid Alqahtani (WSU), Brian A. Collins (WSU), Christina Cheng (Stanford), Valerie Niemann (Stanford), Michael F. Toney (SSRL), Detlef M. Smilgies (Cornell), and Reece Henry (NCSU). We are also grateful to the expert reviewers who patiently guided us repeatedly towards a more correct, complete, and useful manuscript.

References

1. M. Nikolka, I. Nasrallah, B. Rose, M. K. Ravva, K. Broch, A. Sadhanala, D. Harkin, J. Charmet, M. Hurhangee, A. Brown, S. Illig, P. Too, J. Jongman, I. McCulloch, J.-L. Bredas and H. Sirringhaus, *Nat. Mater.*, 2017, **16**, 356-362.
2. A. C. Arias, J. D. MacKenzie, I. McCulloch, J. Rivnay and A. Salleo, *Chem. Rev.*, 2010, **110**, 3-24.
3. D. Abbaszadeh, A. Kunz, G. A. H. Wetzelaer, J. J. Michels, N. I. Craciun, K. Koynov, I. Lieberwirth and P. W. M. Blom, *Nat. Mater.*, 2016, **15**, 628-633.
4. J. L. Bredas, J. E. Norton, J. Cornil and V. Coropceanu, *Acc. Chem. Res.*, 2009, **42**, 1691-1699.
5. Y. X. Li, X. Guo, Z. X. Peng, B. N. Qu, H. P. Yan, H. Ade, M. J. Zhang and S. R. Forrest, *P Natl Acad Sci USA*, 2020, **117**, 21147-21154.

6. E. Ravishankar, R. E. Booth, C. Saravitz, H. Sederoff, H. W. Ade and B. T. O'Connor, *Joule*, 2020, **4**, 490-506.
7. J. Rivnay, S. Inal, A. Salleo, R. M. Owens, M. Berggren and G. G. Malliaras, *Nat Rev Mater*, 2018, **3**, 17086.
8. R. Green and M. R. Abidian, *Adv. Mater.*, 2015, **27**, 7620-7637.
9. S. Inal, J. Rivnay, A. O. Suiu, G. G. Malliaras and I. McCulloch, *Acc. Chem. Res.*, 2018, **51**, 1368-1376.
10. M. A. Rahman, P. Kumar, D. S. Park and Y. B. Shim, *Sensors-Basel*, 2008, **8**, 118-141.
11. K. Fidanovski and D. Mawad, *Adv. Healthcare Mater.*, 2019, **8**, 1900053.
12. J. Rivnay, R. M. Owens and G. G. Malliaras, *Chem. Mater.*, 2014, **26**, 679-685.
13. A. J. Petty, R. L. Keate, B. Jiang, G. A. Ameer and J. Rivnay, *Chem. Mater.*, 2020, **32**, 4095-4115.
14. Y. Tuchman, T. N. Mangoma, P. Gkoupidenis, Y. van de Burgt, R. A. John, N. Mathews, S. E. Shaheen, R. Daly, G. G. Malliaras and A. Salleo, *MRS Bull.*, 2020, **45**, 619-630.
15. Y. van de Burgt, E. Lubberman, E. J. Fuller, S. T. Keene, G. C. Faria, S. Agarwal, M. J. Marinella, A. A. Talin and A. Salleo, *Nat. Mater.*, 2017, **16**, 414-418.
16. P. Corradini, F. Auriemma and C. De Rosa, *Acc. Chem. Res.*, 2006, **39**, 314-323.
17. N. D. Treat, P. Westacott and N. Stingelin, *Annu. Rev. Mater. Res.*, 2015, **45**, 459-490.
18. K. D. Deshmukh, S. K. K. Prasad, N. Chandrasekaran, A. C. Y. Liu, E. Gann, L. Thomsen, D. Kabra, J. M. Hodgkiss and C. R. McNeill, *Chem. Mater.*, 2017, **29**, 804-816.
19. Y. Zhong, M. T. Trinh, R. S. Chen, G. E. Purdum, P. P. Khlyabich, M. Sezen, S. Oh, H. M. Zhu, B. Fowler, B. Y. Zhang, W. Wang, C. Y. Nam, M. Y. Sfeir, C. T. Black, M. L. Steigerwald, Y. L. Loo, F. Ng, X. Y. Zhu and C. Nuckolls, *Nat. Commun.*, 2015, **6**, 8242.
20. Y. C. Hsiao, T. Wu, M. X. Li, W. Qin, L. P. Yu and B. Hu, *Nano Energy*, 2016, **26**, 595-602.
21. S. E. Root, M. A. Alkhadra, D. Rodriquez, A. D. Printz and D. J. Lipomi, *Chem. Mater.*, 2017, **29**, 2646-2654.
22. S. V. Meille, G. Allegra, P. H. Geil, J. S. He, M. Hess, J. I. Jin, P. Kratochvil, W. Mormann and R. Stepto, *Pure Appl. Chem.*, 2011, **83**, 1831-1871.
23. J. Rivnay, S. C. B. Mannsfeld, C. E. Miller, A. Salleo and M. F. Toney, *Chem. Rev.*, 2012, **112**, 5488-5519.
24. J. Rivnay, R. Noriega, R. J. Kline, A. Salleo and M. F. Toney, *Phys Rev B*, 2011, **84**, 045203.
25. A. Hexemer and P. Muller-Buschbaum, *Iucrj*, 2015, **2**, 106-125.
26. J. H. Carpenter, M. Ghasemi, E. Gann, I. Angunawela, S. J. Stuard, J. J. Rech, E. Ritchie, B. T. O'Connor, J. Atkin, W. You, D. M. DeLongchamp and H. Ade, *Adv. Funct. Mater.*, 2019, **29**, 1806977.
27. R. Noriega, J. Rivnay, K. Vandewal, F. P. V. Koch, N. Stingelin, P. Smith, M. F. Toney and A. Salleo, *Nat. Mater.*, 2013, **12**, 1038-1044.
28. A. Salleo, *Mater. Today*, 2007, **10**, 38-45.
29. D. W. V. Krevelen and K. T. Nijenhuis, *Properties of polymers*, Elsevier Science, 2009.
30. X. P. Xu, T. Yu, Z. Z. Bi, W. Ma, Y. Li and Q. Peng, *Adv. Mater.*, 2018, **30**, 1703973.
31. B. B. Fan, L. Ying, P. Zhu, F. L. Pan, F. Liu, J. W. Chen, F. Huang and Y. Cao, *Adv. Mater.*, 2017, **29**, 1703906.
32. L. Ye, Y. Xiong, H. F. Yao, A. Gadisa, H. Zhang, S. S. Li, M. Ghasemi, N. Balar, A. Hunt, B. T. O'Connor, J. H. Hou and H. Ade, *Chem. Mater.*, 2016, **28**, 7451-7458.
33. X. C. Jiao, L. Ye and H. Ade, *Adv. Energy Mater.*, 2017, **7**, 1700084.
34. W. Ma, G. F. Yang, K. Jiang, J. H. Carpenter, Y. Wu, X. Y. Meng, T. McAfee, J. B. Zhao, C. H. Zhu, C. Wang, H. Ade and H. Yan, *Adv. Energy Mater.*, 2015, **5**, 1501400.
35. Z. X. Peng, X. C. Jiao, L. Ye, S. S. Li, J. J. Rech, W. You, J. H. Hou and H. Ade, *Chem. Mater.*, 2018, **30**, 3943-3951.
36. J. Clark, C. Silva, R. H. Friend and F. C. Spano, *Phys. Rev. Lett.*, 2007, **98**, 206406.
37. N. J. Hestand and F. C. Spano, *Chem. Rev.*, 2018, **118**, 7069-7163.

38. D. T. Duong, M. F. Toney and A. Salleo, *Phys Rev B*, 2012, **86**, 205205.
39. D. T. Duong, V. Ho, Z. R. Shang, S. Mollinger, S. C. B. Mannsfeld, J. Dacuna, M. F. Toney, R. Segalman and A. Salleo, *Adv. Funct. Mater.*, 2014, **24**, 4515-4521.
40. A. Salleo, R. J. Kline, D. M. DeLongchamp and M. L. Chabinyc, *Adv. Mater.*, 2010, **22**, 3812-3838.
41. I. Mcculloch, M. Heeney, C. Bailey, K. Genevicius, I. Macdonald, M. Shkunov, D. Sparrowe, S. Tierney, R. Wagner, W. M. Zhang, M. L. Chabinyc, R. J. Kline, M. D. Mcgehee and M. F. Toney, *Nat. Mater.*, 2006, **5**, 328-333.
42. M. Grell, M. Redecker, K. S. Whitehead, D. D. C. Bradley, M. Inbasekaran, E. P. Woo and W. Wu, *Liq. Cryst.*, 1999, **26**, 1403-1407.
43. M. Heeney, C. Bailey, M. Giles, M. Shkunov, D. Sparrowe, S. Tierney, W. M. Zhang and I. McCulloch, *Macromolecules*, 2004, **37**, 5250-5256.
44. N. Zhao, G. A. Botton, S. P. Zhu, A. Duft, B. S. Ong, Y. L. Wu and P. Liu, *Macromolecules*, 2004, **37**, 8307-8312.
45. R. X. Xie, M. P. Aplan, N. J. Caggiano, A. R. Weisen, T. Su, C. Muller, M. Segad, R. H. Colby and E. D. Gomez, *Macromolecules*, 2018, **51**, 10271-10284.
46. X. R. Zhang, S. D. Hudson, D. M. DeLongchamp, D. J. Gundlach, M. Heeney and I. McCulloch, *Adv. Funct. Mater.*, 2010, **20**, 4098-4106.
47. B. A. Collins, J. E. Cochran, H. Yan, E. Gann, C. Hub, R. Fink, C. Wang, T. Schuettfort, C. R. McNeill, M. L. Chabinyc and H. Ade, *Nat. Mater.*, 2012, **11**, 536-543.
48. E. Gann, B. A. Collins, M. L. Tang, J. R. Tumbleston, S. Mukherjee and H. Ade, *J Synchrotron Radiat*, 2016, **23**, 219-227.
49. H. Ade and B. Hsiao, *Science*, 1993, **262**, 1427-1429.
50. P. U. P. A. Gilbert, *Microsc. Microanal.*, 2018, **24**, 454-457.
51. J. Balko, G. Portale, R. H. Lohwasser, M. Thelakkat and T. Thurn-Albrecht, *J Mater Res*, 2017, **32**, 1957-1968.
52. N. Stribeck, *X-Ray Scattering of Soft Matter*, Springer Berlin Heidelberg, New York, **2007**.
53. B. E. Warren, *X-Ray Diffraction*, Dover Publications, Inc., New York, **1990**.
54. J. L. Baker, L. H. Jimison, S. Mannsfeld, S. Volkman, S. Yin, V. Subramanian, A. Salleo, A. P. Alivisatos and M. F. Toney, *Langmuir*, 2010, **26**, 9146-9151.
55. L. H. Jimison, *Understanding microstrucutre and charge transport in semicrystalline polythiophenes*, Ph. D. Thesis, Stanford University, Stanford, CA, **2011**.
56. S. C. B. Mannsfeld, A. Virkar, C. Reese, M. F. Toney and Z. N. Bao, *Adv. Mater.*, 2009, **21**, 2294-2298.
57. D. M. DeLongchamp, R. J. Kline and A. Herzing, *Energ Environ Sci*, 2012, **5**, 5980-5993.
58. P. Brocorens, A. Van Vooren, M. L. Chabinyc, M. F. Toney, M. Shkunov, M. Heeney, I. McCulloch, J. Cornil and R. Lazzoroni, *Adv. Mater.*, 2009, **21**, 1193-1198.
59. B. W. Boudouris, V. Ho, L. H. Jimison, M. F. Toney, A. Salleo and R. A. Segalman, *Macromolecules*, 2011, **44**, 6653-6658.
60. L. H. Jimison, A. Salleo, M. L. Chabinyc, D. P. Bernstein and M. F. Toney, *Phys Rev B*, 2008, **78**, 125319.
61. J. A. Merlo, C. R. Newman, C. P. Gerlach, T. W. Kelley, D. V. Muyres, S. E. Fritz, M. F. Toney and C. D. Frisbie, *J. Am. Chem. Soc.*, 2005, **127**, 3997-4009.
62. A. K. Hailey, A. M. Hiszpanski, D. M. Smilgies and Y. L. Loo, *J Appl Crystallogr*, 2014, **47**, 2090-2099.
63. D. M. Smilgies, *J Appl Crystallogr*, 2009, **42**, 1030-1034.
64. J. I. Langford and A. J. C. Wilson, *J Appl Crystallogr*, 1978, **11**, 102-113.
65. N. Morosoff, K. Sakaoku and A. Peterlin, *J. Polym. Sci. B Polym. Phys.*, 1972, **10**, 1221-1236.
66. R. Hosemann, M. P. Hentschel, F. J. Balta-Calleja, E. Lopez Cabarcos and A. M. Hindeleh, *J. Phys. C: Solid State Phys.*, 1985, **18**, 961-971.
67. W. Vogel and R. Hosemann, *Acta Cryst.*, 1970, **A 26**, 272.

68. R. Hosemann and S. N. Bagchi, *Direct analysis of diffraction by matter*, North Holland Publ Comp, Amsterdam, **1962**.
69. B. E. Warren and B. L. Averbach, *J Appl Phys*, 1952, **23**, 497-497.
70. B. E. Warren and B. L. Averbach, *J Appl Phys*, 1950, **21**, 595-599.
71. T. J. Prosa, J. Moulton, A. J. Heeger and M. J. Winokur, *Macromolecules*, 1999, **32**, 4000-4009.
72. G. K. Williamson and W. H. Hall, *Acta Metall Mater*, 1953, **1**, 22-31.
73. X. Jiao, M. Statz, L. Lai, S. Schott, C. Jellett, I. McCulloch, H. Sirringhaus and C. R. McNeill, *J. Phys. Chem. B*, 2020, **124**, 10529-10538.
74. I. Lucks, P. Lamparter and E. J. Mittemeijer, *J Appl Crystallogr*, 2004, **37**, 300-311.
75. X. B. Shen, W. G. Hu and T. P. Russell, *Macromolecules*, 2016, **49**, 4501-4509.
76. C. R. Snyder, R. C. Nieuwendaal, D. M. DeLongchamp, C. K. Luscombe, P. Sista and S. D. Boyd, *Macromolecules*, 2014, **47**, 3942-3950.
77. J. M. Goppel and J. J. Arlman, *Appl. Sci. Res.*, 1949, **1**, 462-474.
78. A. Weidinger and P. H. Hermans, *Makromol. Chem.*, 1961, **50**, 98-115.
79. J. Balko, R. H. Lohwasser, M. Sommer, M. Thelakkat and T. Thurn-Albrecht, *Macromolecules*, 2013, **46**, 9642-9651.
80. O. F. Pascui, R. Lohwasser, M. Sommer, M. Thelakkat, T. Thurn-Albrecht and K. Saalwachter, *Macromolecules*, 2010, **43**, 9401-9410.
81. E. Hunter and W. G. Oakes, *Trans. Farad. Soc.*, 1945, **41**, 49-56.
82. N. Kayunkid, S. Uttiya and M. Brinkmann, *Macromolecules*, 2010, **43**, 4961-4967.
83. J. Rivnay, L. H. Jimison, J. E. Northrup, M. F. Toney, R. Noriega, S. Lu, T. J. Marks, A. Facchetti and A. Salleo, *Nat. Mater.*, 2009, **8**, 952-958.
84. B. Grevin, P. Rannou, R. Payerne, A. Pron and J. P. Travers, *Adv. Mater.*, 2003, **15**, 881-884.
85. R. A. Street, J. E. Northrup and A. Salleo, *Phys Rev B*, 2005, **71**, 165202.
86. X. Guo, Q. P. Fan, J. N. Wu, G. W. Li, Z. X. Peng, W. Y. Su, J. Lin, L. T. Hou, Y. P. Qin, H. Ade, L. Ye, M. J. Zhang and Y. F. Li, *Angew. Chem. Int. Edit.*, 2021, **60**, 2322-2329.
87. J. R. Tumbleston, B. A. Collins, L. Q. Yang, A. C. Stuart, E. Gann, W. Ma, W. You and H. Ade, *Nat. Photonics*, 2014, **8**, 385-391.
88. M. Schubert, B. A. Collins, H. Mangold, I. A. Howard, W. Schindler, K. Vandewal, S. Roland, J. Behrends, F. Kraffert, R. Steyrleuthner, Z. H. Chen, K. Fostiropoulos, R. Bittl, A. Salleo, A. Facchetti, F. Laquai, H. W. Ade and D. Neher, *Adv. Funct. Mater.*, 2014, **24**, 4068-4081.
89. A. Hexemer, W. Bras, J. Glossinger, E. Schaible, E. Gann, R. Kirian, A. MacDowell, M. Church, B. Rude and H. Padmore, *J. Phys.: Conf. Ser.*, 2010, **247**, 012007.
90. X. H. Lu, H. Hlaing, D. S. Germack, J. Peet, W. H. Jo, D. Andrienko, K. Kremer and B. M. Ocko, *Nat. Commun.*, 2012, **3**, 795.
91. M. L. Chabinyc, M. F. Toney, R. J. Kline, I. McCulloch and M. Heeney, *J. Am. Chem. Soc.*, 2007, **129**, 3226-3237.
92. J. Chen, J. Anthony and D. C. Martin, *J. Phys. Chem. B*, 2006, **110**, 16397-16403.
93. J. B. Sherman, K. Moncino, T. Baruah, G. Wu, S. R. Parkin, B. Purushothaman, R. Zope, J. Anthony and M. L. Chabinyc, *J. Phys. Chem. C*, 2015, **119**, 20823-20832.
94. G. W. Ehrenstein and R. P. Theriault, *Polymeric Materials: Structure, Properties, Applications*, Hanser Publishers, 2001.
95. D. M. Smilgies, *J Appl Crystallogr*, 2019, **52**, 247-251.
96. A. Charlesby, *J. Polym. Sci.*, 1953, **10**, 201-211.
97. C. R. Snyder and D. M. DeLongchamp, *Curr. Opin. Solid State Mater. Sci*, 2018, **22**, 41-48.
98. M. D. Ediger and P. Harrowell, *J. Chem. Phys.*, 2012, **137**, 080901.
99. M. D. Ediger, J. de Pablo and L. Yu, *Acc. Chem. Res.*, 2019, **52**, 407-414.
100. Z. Y. Qian, L. Galuska, W. W. McNutt, M. U. Ocheje, Y. J. He, Z. Q. Cao, S. Zhang, J. Xu, K. L. Hong, R. B. Goodman, S. Rondeau-Gagne, J. G. Mei and X. D. Gu, *J. Polym. Sci. B Polym. Phys.*, 2019, **57**, 1635-1644.

101. K. Vakhshouri, B. H. Smith, E. P. Chan, C. C. Wang, A. Salleo, C. Wang, A. Hexemer and E. D. Gomez, *Macromolecules*, 2016, **49**, 7359-7369.
102. M. Brinkmann and P. Rannou, *Adv. Funct. Mater.*, 2007, **17**, 101-108.
103. T. J. Prosa, M. J. Winokur, J. Moulton, P. Smith and A. J. Heeger, *Macromolecules*, 1992, **25**, 4364-4372.
104. R. R. Lunt, J. B. Benziger and S. R. Forrest, *Adv. Mater.*, 2010, **22**, 1233-1236.
105. X. H. Jin, M. B. Price, J. R. Finnegan, C. E. Boott, J. M. Richter, A. Rao, M. Menke, R. H. Friend, G. R. Whittell and I. Manners, *Science*, 2018, **360**, 897-900.
106. X. B. Shen, V. V. Duzhko and T. P. Russell, *Adv. Energy Mater.*, 2013, **3**, 263-270.
107. A. T. Yiu, P. M. Beaujuge, O. P. Lee, C. H. Woo, M. F. Toney and J. M. J. Frechet, *J. Am. Chem. Soc.*, 2012, **134**, 2180-2185.
108. W. T. Li, S. Abrecht, L. Q. Yang, S. Roland, J. R. Tumbleston, T. McAfee, L. Yan, M. A. Kelly, H. Ade, D. Neher and W. You, *J. Am. Chem. Soc.*, 2014, **136**, 15566-15576.
109. J. Liu, H. T. Zhang, H. L. Dong, L. Q. Meng, L. F. Jiang, L. Jiang, Y. Wang, J. S. Yu, Y. M. Sun, W. P. Hu and A. J. Heeger, *Nat. Commun.*, 2015, **6**, 10032.
110. R. Steyrleuthner, R. Di Pietro, B. A. Collins, F. Polzer, S. Himmelberger, M. Schubert, Z. H. Chen, S. M. Zhang, A. Salleo, H. Ade, A. Facchetti and D. Neher, *J. Am. Chem. Soc.*, 2014, **136**, 4245-4256.
111. D. M. DeLongchamp, R. J. Kline, Y. Jung, E. K. Lin, D. A. Fischer, D. J. Gundlach, S. K. Cotts, A. J. Moad, L. J. Richter, M. F. Toney, M. Heeney and I. McCulloch, *Macromolecules*, 2008, **41**, 5709-5715.
112. M. A. Brady, G. M. Su and M. L. Chabinyc, *Soft Matter*, 2011, **7**, 11065-11077.
113. H. G. Kim, B. Kang, H. Ko, J. Lee, J. Shin and K. Cho, *Chem. Mater.*, 2015, **27**, 829-838.
114. K. Weiss, H. Ostrom, L. Triguero, H. Ogasawara, M. G. Garnier, L. G. M. Pettersson and A. Nilsson, *J. Electron Spectrosc.*, 2003, **128**, 179-191.
115. C. Muller, M. Aghamohammadi, S. Himmelberger, P. Sonar, M. Garriga, A. Salleo and M. Campoy-Quiles, *Adv. Funct. Mater.*, 2013, **23**, 2368-2377.
116. L. H. Jimison, M. F. Toney, I. McCulloch, M. Heeney and A. Salleo, *Adv. Mater.*, 2009, **21**, 1568-1572.
117. B. Kang, R. Kim, S. B. Lee, S. K. Kwon, Y. H. Kim and K. Cho, *J. Am. Chem. Soc.*, 2016, **138**, 3679-3686.
118. K. S. Ahn, H. Jo, J. B. Kim, I. Seo, H. H. Lee and D. R. Lee, *Acs Appl. Mater. Interfaces*, 2020, **12**, 1142-1150.
119. R. J. Kline, D. M. DeLongchamp, D. A. Fischer, E. K. Lin, L. J. Richter, M. L. Chabinyc, M. F. Toney, M. Heeney and I. McCulloch, *Macromolecules*, 2007, **40**, 7960-7965.
120. D. A. Warr, L. M. A. Perdigao, H. Pinfold, J. Blohm, D. Stringer, A. Leventis, H. Bronstein, A. Troisi and G. Costantini, *Sci. Adv.*, 2018, **4**.
121. D. Venkateshvaran, M. Nikolka, A. Sadhanala, V. Lemaur, M. Zelazny, M. Kepa, M. Hurhangee, A. J. Kronemeijer, V. Pecunia, I. Nasrallah, I. Romanov, K. Broch, I. McCulloch, D. Emin, Y. Olivier, J. Cornil, D. Beljonne and H. Sirringhaus, *Nature*, 2014, **515**, 384-388.
122. R. Colle, G. Grosso, A. Ronzani and C. M. Zicovich-Wilson, *Phys. Status Solidi B*, 2011, **248**, 1360-1368.
123. M. Brinkmann and P. Rannou, *Macromolecules*, 2009, **42**, 1125-1130.
124. N. Norman and M. H., *Acta Chem. Scand.*, 1961, **15**, 1755-1760.
125. E. Cho, C. Risko, D. Kim, R. Gysel, N. C. Miller, D. W. Breiby, M. D. McGehee, M. F. Toney, R. J. Kline and J. L. Bredas, *J. Am. Chem. Soc.*, 2012, **134**, 6177-6190.
126. S. C. Nyburg, F. M. Pickard and N. Norman, *Acta Cryst. B*, 1976, **32**, 2289.